Edinburgh Research Explorer

Modelling the formation of explosively formed projectiles (EFP)

OPEN ACCESS

Corresponding Author: Dr. Filipe Teixeira-Dias, BEng, MSc, PhD, Hab

Corresponding Author's Institution: University of Edinburgh

First Author: Diogo Cardoso

Order of Authors: Diogo Cardoso; Filipe Teixeira-Dias, BEng, MSc, PhD, Hab

Abstract: The number of victims of attacks from Improvised Explosive Devices (IED), especially from roadside bombs where Explosively Formed Projectiles (EFP) are frequently used, has steeply increased until 2011. Understanding these threats, how they are built and predicting how they interact with targets is of utmost importance. For this purpose it is first necessary to understand how EFPs are formed and what parameters influence their behaviour and performance. The work in this paper proposes and describes a numerical simulation methodology that allows to reproduce the conditions of formation and ballistic capabilities of explosively formed projectiles. Different EFP configurations, materials and detonation conditions are evaluated and assessed against the performance (e.g. stable flight velocity) of the resulting projectile. The model proposed is based on a generic EFP with an aspect ratio of approximately 1 and a case/base thickness of 5 mm. The dynamic interactions between the various components of the EFP are established through specific contact algorithms that allow to interpolate the resulting pressure from detonation to the remaining components, resulting in their acceleration and consequent deformation. The model is validated against experimental observations and afterwards used to assess the influence of the liner materials and thickness, high-explosive, number and off-centre distance of detonators. The performance of the EFPs is quantified from their configuration and a set of non-dimensional geometrical parameters. It is shown that the thickness (and thickness variability) of the liner is one of the most important factors, along with the off-centre distance of the detonator(s). Within the materials and range of parameters tested, the most performant and aggressive EFP has a liner with thickness between 4 and 7% of its diameter, a copper liner and dynamite high-explosive (HE).

Cover Letter

SCHOOL *of* ENGINEERING

INSTITUTE *for* INFRASTRUCTURE *and* ENVIRONMENT
The University of Edinburgh
Alexander Graham Bell Building
The King's Buildings
Edinburgh EH9 3JL
Scotland, UK
Tel: +44 (0)131 650 6768
Fax : +44 (0)131 650 6554
Email: F.Teixeira-Dias@ed.ac.uk

Dear Professor Magnus Langseth,
Editor-in-Chief of the International Journal of Impact Engineering,

Please find attached to this cover letter the manuscript entitled *Modelling the formation of Explosively Formed Projectiles (EFP)*, from the authors D. Cardoso and F. Teixeira-Dias.

The work in this manuscript proposes, describes and validates a numerical simulation methodology that allows to reproduce the conditions of formation and ballistic capabilities of explosively formed projectiles (EFP). Different EFP configurations, materials and detonation conditions are evaluated and assessed against the performance (*e.g.* stable flight velocity) of the resulting projectiles. The model proposed is based on a generic EFP, is validated against experimental observations and used to assess the influence of the liner materials and thickness, high-explosive, number and off-centre distance of detonators on the performance of the EFP, quantified from their configuration and a set of non-dimensional geometrical parameters.

We hope that this paper can be accepted for publication in the International Journal of Impact Engineering.

With best wishes,

The University of Edinburgh, 1 June 2015

_____

Filipe Teixeira-Dias

Title

Modelling the formation of Explosively Formed Projectiles (EFP)

Authors

D. Cardoso, F. Teixeira-Dias

Submitted to

International Journal of Impact Engineering

Date

1 June 2015

Highlights

- Authors model the formation process of explosively formed projectiles.
- Study influence of materials (liner, HE) and detonation parameters.
- Stable flight velocity is strongly influenced by liner thickness variability.
- Kinetic energy of resulting projectile highly dependent on detonation parameters.

Modelling the formation of Explosively Formed Projectiles (EFP)

D. Cardoso[a], F. Teixeira-Dias[b,*]

[a]*GRIDS, Universidade de Aveiro, Portugal*
[b]*School of Engineering, The University of Edinburgh, Edinburgh EH9 3JL, UK*

Abstract

The number of victims of attacks from Improvised Explosive Devices (IED), especially from roadside bombs where Explosively Formed Projectiles (EFP) are frequently used, has steeply increased until 2011. Understanding these threats, how they are built and predicting how they interact with targets is of utmost importance. For this purpose it is first necessary to understand how EFPs are formed and what parameters influence their behaviour and performance. The work in this paper proposes and describes a numerical simulation methodology that allows to reproduce the conditions of formation and ballistic capabilities of explosively formed projectiles. Different EFP configurations, materials and detonation conditions are evaluated and assessed against the performance (*e.g.* stable flight velocity) of the resulting projectile. The model proposed is based on a generic EFP with an aspect ratio of approximately 1 and a case/base thickness of 5 mm. The dynamic interactions between the various components of the EFP are established through specific contact algorithms that allow to interpolate the resulting pressure from detonation to the remaining components, resulting in their

acceleration and consequent deformation. The model is validated against experimental observations and afterwards used to assess the influence of the liner materials and thickness, high-explosive, number and off-centre distance of detonators. The performance of the EFPs is quantified from their configuration and a set of non-dimensional geometrical parameters. It is shown that the thickness (and thickness variability) of the liner is one of the most important factors, along with the off-centre distance of the detonator(s). Within the materials and range of parameters tested, the most performant and aggressive EFP has a liner with thickness between 4 and 7% of its diameter, a copper liner and dynamite high-explosive (HE).

Keywords: Explosively formed projectile; EFP; improvised explosive device; IED; high strain-rate; detonation; projectile; finite element method.

1. Introduction and state-of-the-art

Shock waves from the detonation of an high-explosive (HE) can be used to deform and warp a liner of ductile metal, forming Explosively Formed Projectiles (EFP), also known as Self-Forging Fragments (SFF). These compact projectiles can reach velocities in excess of 1000 m/s, with the consequent kinetic energy.

The first publications with reference to devices similar to present-day EFPs appeared in 1935 [1] and 1936 [2]. However, it was not until the 1970s that related studies significantly increased. Johnson [3] firstly demonstrated

*Corresponding author: F.Teixeira-Dias@ed.ac.uk

the existence of three-dimensional numerical modelling capabilities of the explosive-metal interaction using complex surfaces. To this end, this author used the example of an explosive that accelerates a metal projectile after detonation. This study investigated: (i) the effect of shell (liner) thickness, from $0.9t_0$ at the edge of the liner up to $1.1t_0$ in its centre (t_0 being the thickness of a projectile with an equivalent mass), (ii) the effect of an off-centre detonation and (iii) the effect of an uneven distribution of the density of the high explosive. It was shown that these parameters significantly influence the stable flight velocity of the projectile. More recently, Johnson [4] explored issues related to modelling three-dimensional EFP, explaining the effects of the contact interface, discretisation and finite element approach. Similar computational topics were extensively researched by Zukas *et al.* [5], Taylor [6], Nyström *et al.* [7] and Molinari [8], focusing on aspects such as the effect of meshing, blast load intensity, constitutive modelling and the use of alternative methods (*e.g.* Smooth Particle Hydrodynamics, SPH).

Geometrical parameters are known to play an important role on the formation of an EFP. Miller [9] and Brown *et al.* [10] provided a set of EFP design criteria based on projectile velocity or mass concentration. Weickert *et al.* [11] and Chuan *et al.* [12] discuss different design approaches, focusing on target penetration. One of the most significant and influential parameters is the aspect ratio (length-to-diameter ratio) of the explosive before detonation, which led Bender and Carleone [13] to conclude that the kinetic energy of the projectile increases with this ratio up to a maximum

3

of 1.5. Another important observation was the effect of adding mass to the casing, increasing the duration of the shock wave propagation and consequently the total energy transferred to the projectile. Weimann [14] and Weickert and Gallagher [15] demonstrated that adding a reinforcement ring to the case and liner has a significant effect on the shape, configuration and velocity of the resulting EFP, eventually even providing fins that aerodynamically stabilise the projectile during its flight. Bender and Carleone [16] submitted a patent in 1994 explaining the use of a thin radial spacer between the projectile and the high-explosive, leading to periodic thickness variations and, consequently, the formation of fins.

Pappu and Murr [17] analysed, both experimentally and numerically, the characteristics of residual microstructures of several EFPs, testing three different liner materials (tantalum, iron and copper) using two constitutive models for each material (Johnson-Cook [18, 19] and Zerilli-Armstrong [20]). They concluded that, although the selected materials have been widely used in EFP [21, 22, 23, 24], they lead to completely distinct behaviour, influencing the melting temperature and the mechanisms by which the crystal structure deforms. The Zerilli-Armstrong model [20] led to better results for tantalum (Ta) projectiles, unlike iron (Fe) that exhibited better results with the Johnson-Cook model. Results were similar, however, for the copper (Cu) projectiles.

More recently, Wu *et al.* [25] studied the formation, flight and penetration performance of EFPs using a single geometric configuration with an

Arbitrary Lagrangian-Eulerian (ALE) approach. These authors considered air drag during flight through an attenuation rate equation for a fixed flight distance (of 48 m). The projectile velocity was analysed both with the similarity theory and the numerical simulation results, which were validated by experimental residual velocity measurements after impact on a 25 mm ballistic steel target. It was concluded that it is still possible to optimise the geometry of the EFP by combining the shape of the explosive and liner. As simulating the flight of the EFP is complex and impractical, only 0.5 m of flight were analysed, nonetheless leading to reasonably accurate results. The attenuation method can be considered accurate, with a loss of speed of approximately 6.4 m/s per meter of flight, consistent with the experimental results. The use of the similarity theory can be useful to solve technical problems associated to the determination of the entire flight of the EFP: the error obtained on the residual velocity for a 0.5 m flight is lower than 10%. Finally, by comparing the velocity and penetration on the target results, Wu *et al.* [25] concluded that simulations can reasonably predict the final shape, mass, velocity, flight stability and penetration performance of an EFP.

Li *et al.* [26] examined the effects of the position, timing and number of detonation points on the formation of the EFP, concluding that the stable flight velocity of the projectile increases with the number of detonation points, observing that for a 60 mm diameter EFP the signal delay between detonators should not be above 200 μs. Experimental results confirm that

5

for certain flight distances the penetration capacity doubles and the perforation diameter reduces by as much as 40%.

According to statistics published by the Center for Strategic & International Studies (CSIS) [27] and data from the US Department of Defense published by The Washington Post in 2011 [28] and 2014 [29], the number of casualties due to Improvised Explosive Devices (IED) in Iraq strongly increased from 2009 to 2010, with increases as high as 60% on some periods. Although these numbers have been dropping steadily since 2010 (IED casualties have dropped by 48% in 2012 alone), IEDs and EFP devices in particular are still, and will remain, a significant threat in years to come. It is thus highly relevant to develop efficient and reliable means of assessing and predicting the behaviour of such devices, in the end leading to the development of technologies, methods and systems that can better protect against them. The main aim of the present paper is then to contribute to this, with a methodology, a finite element modelling approach and formulation, as well as the corresponding formulations, reproducing the conditions of formation and ballistic capabilities of EFPs.

2. Numerical model

2.1. Geometry and boundary conditions

When developing the numerical models, attention was given to the accurate reproduction of the boundary conditions and geometrical configurations. The work of Wu *et al.* [25] was used as reference and for validation

6

purposes. The proposed geometry is that of a generic EFP, as shown in Figure 1, with a length-to-diameter ratio $L/D = 1.07$, liner of diameter $D = 56$ mm, thickness $e = 2$ mm, curvature with radius $R = 120$ mm and sweeping angle $\alpha = 29°$. The casing and the base have thickness $e' = 5$ mm. The remaining dimensions will change according to the specific model being tested. The complexity of the dynamic interactions between the various components of the EFP (*e.g.* explosive-metal interaction) lead to a detailed and costly modelling process. Interactions between the products of detonation and the remaining components of the EFP are defined using a specific contact algorithm that can model surface sliding and is based on a master-slave segments approach. With this algorithm pressure values are interpolated and passed to the remaining components of the EFP, leading to their acceleration and consequent deformation.

The symmetry boundary conditions used in the numerical models are schematically shown in Figure 2. This allows models to run with a significantly lower computational cost. Fully three-dimensional models were used however, where no symmetry is present.

The detonation point — its position and detonation time (*e.g.* see Figure 2) — defines the instant and geometrical coordinates of ignition, dictating the behaviour of the shock wave and the subsequent deformation and flight of the projectile.
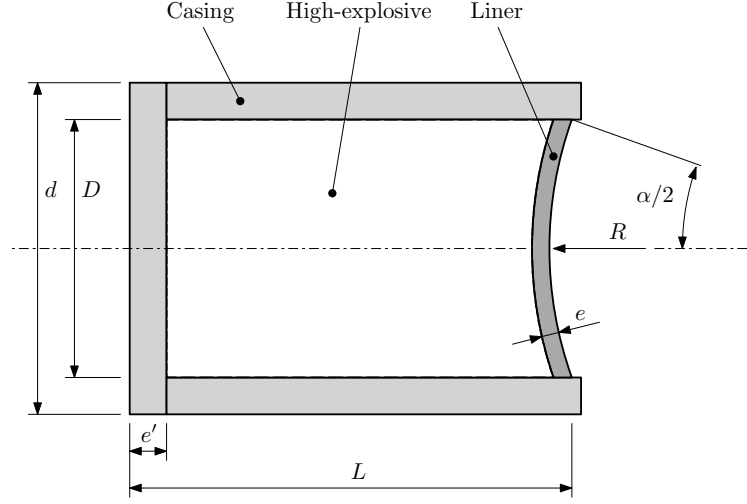
7

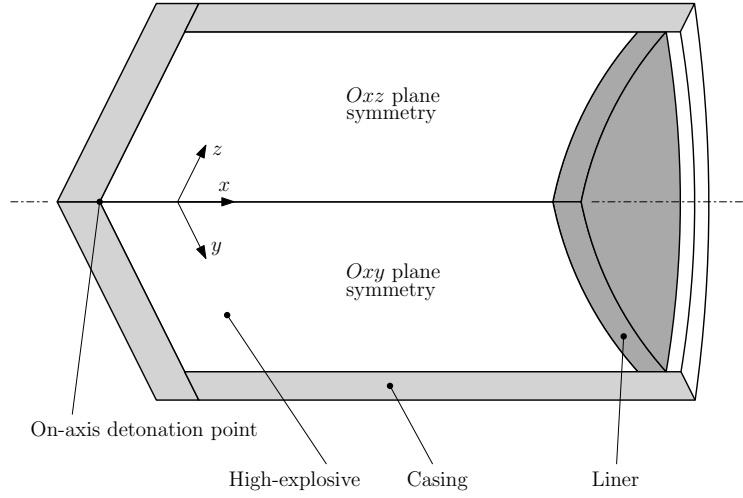Figure 1: Schematic representation of the generic EFP geometry.

Figure 2: Schematic representation of the generic symmetry boundary conditions.

2.2. Material modelling

Different materials were used to allow for the study of different EFP configurations. These include OFHC copper, ARMCO iron and tantalum

as liners; Octal, composition B (CompB) and dynamite as high-explosives; and steel 1006 and aluminium alloy 6061-T6 for the casing and base of the EFP, respectively. The properties of the materials used were validated using numerical and experimental results previously published by other authors, who have studied their behaviour in similar situations and strain rate regimes [17, 18, 25].

Materials are subjected to high pressure, temperature and high deformations and strain-rates during the formation of the EFP. Johnson-Cook's constitutive model was thus chosen as the most appropriate model to predict the high strain rate behaviour of the metallic materials [18, 19]. This constitutive model is the most widely referenced for impact and high strain rate behaviour when triaxial stress states depend on both the deformation rate and temperature. Due to the propagation of shock waves and high pressures involved within the metallic materials it is also necessary to define an equation of state (EOS) along with the Johnson-Cook model. The Johnson-Cook effective stress can be defined as a function of the plastic strain, plastic strain-rate and the temperature, as

$$\bar{\sigma} = (A + B\varepsilon^n) \left[1 + C \ln\left(\dot{\varepsilon}^*\right)\right] \left[1 - (T^*)^m\right] \tag{1}$$

where A, B, C, n and m are the yield stress, the hardening constant, the strain-rate constant, the hardening exponent and the thermal softening coefficient, respectively. The effective plastic strain is $\dot{\varepsilon}^* = \dot{\varepsilon}/\dot{\varepsilon}_0$ and the non-dimensional temperature is $T^* = (T - T_0)/(T_m - T_0)$, T_m is the melting

9

temperature, T_0 is room temperature and T is the current temperature.

The Gruneisen equation of state is used in conjunction with the Johnson-Cook constitutive model. This EOS describes how the materials react to the shock wave and is based on Hugoniot's linear relation between the shock wave velocity, v_s, and the material particle velocity, v_p, as $v_s = c_0 + s v_p$, where c_0 is the wave speed and s is a material parameter. For a dense material, the Gruneisen EOS, which relates pressure p with internal energy E, is

$$p = \rho_0 c_0^2 \mu \Psi + (\gamma_0 + a\mu) E \tag{2}$$

with

$$\Psi = \frac{2 - a\mu^2 + (2 - \gamma_0)\mu}{2\left[1 - (S_1 - 1)\mu - S_2\frac{\mu^2}{1+\mu} - S_3\frac{\mu^3}{(1+\mu)^2}\right]} \tag{3}$$

where γ_0 is the Gruneisen coefficient, a is a first order energy correction factor and S_i $(i = 1, \ldots, 3)$ are material parameters. $\mu = \rho/\rho_0 - 1$ is an non-dimensional coefficient based on the initial and instantaneous material densities [30]. All material properties are listed in Table 1.

The behaviour of the high-explosives can be characterised by the Jones-Wilkins-Lee (JWL) equation of state that describes the pressure-volume relationship associated with a detonation process [33, 34, 35], which is based on the Gruneisen EOS, adjusted with experimental data. As with other empirical equations of state, viscosity, conductivity, friction and field forces (*i.e.* gravity) are neglected. The practical nature and large experimental data base supported by this EOS are two major advantages over alternative

Table 1: Material properties for the Johnson-Cook constitutive model and Gruneisen and Jones-Wilkins-Lee equations of state [17, 18, 25, 31, 32].

Property	OFHC Copper	ARMCO Iron	Tantalum	Steel 1006	Aluminum 6061-T6
ρ [kg/m^3]	8930	7890	16690	7896	2785
A [GPa]	0.12	1	0.8	0.35	0.265
B [GPa]	0.2	0.38	0.55	0.275	0.426
C	0.04	0.06	0.0575	0.022	0.015
n	0.15	0.31	0.4	0.36	0.34
m	0.55	0.55	0.44	1	1
T_m [K]	1360	1812	3293	1811	775
T_0 [K]	293	293	293	293	293
c_0 [m/s]	3940	3630	3400	4569	5328
S_1	1.49	1.8	1.17	1.49	1.338
S_2	0.0	0.0	0.074	0.0	0.0
S_3	0.0	0.0	-0.038	0.0	0.0
γ_0	1.99	1.81	1.6	2.17	2.0

	Dynamite	CompB	Octol
ρ [kg/m^3]	1680	1717	1821
A [GPa]	852.4	524.23	748.6
B [GPa]	18.02	7.678	13.38
R_1	4.55	4.2	4.5
R_2	1.3	1.1	1.2
ω	0.38	0.34	0.38
E [kJ/m^3]	8.5	8.5	9.6
V_0	1	1	1

EOS. The JWL equation of state can be described by

$$p = A' \left(1 - \frac{\omega}{R_1 V^*}\right) e^{-R_1 V^*} + B' \left(1 - \frac{\omega}{R_2 V^*}\right) e^{-R_2 V^*} + \frac{\omega E}{V^*}. \qquad (4)$$

This expression relates pressure p with relative volume $V^* = V/V_0$ and the energy E, where V_0 is the initial volume of unreacted explosive and V is the

volume of material under pressure. The energy term accounts both for the chemical and the kinetic energies associated with the detonation. Constants A', B', R_1, R_2 and ω are the pressure coefficients, the first and second eigenvalues and the fractional part of the adiabatic exponent, respectively [36].

2.3. Model validation

The work of Wu *et al.* [25] is used as the basis for validation of the numerical models proposed in this paper. The approach in the present work is purely Lagrangian and does not consider any aerodynamic effects on the projectile (*i.e.* drag and lift forces). However, the experimental velocities observed by Wu *et al.* were measured after 48 m of flight. It was then necessary to account for these differences objectively on the validation procedure.

The generic dimensions of the model used for validation, as defined in Figure 1, are diameter $d = 60$ mm, liner diameter $D = 56$ mm and length $L = 66$ mm . Wu *et al.* [25] do not provide detailed information about the exact thickness of the liner used in their experiments. These authors only refer that it is within 1 to 8% of the diameter of the EFP. Consequently, the thickness chosen to be used in the validation model is 5% of the diameter, that is, $e = 3$ mm.

The experimentally measured velocity for this device was $v_{\mathrm{x}} = 1267$ m/s, at a distance $D_{\mathrm{f}} = 48$ m from the detonation position [25]. Additionally, and still according to Wu *et al.*, the average velocity decrease with distance due to aerodynamic drag is approximately $\alpha = 6.4$ m/s per meter of flight.

12

Applying this velocity attenuation factor to the numerical results here presented, the stable flight velocity immediately after the projectile formation stage should be within the range of velocities defined by

$$v_f = v_x(1 \pm \lambda) + \alpha D_f \tag{5}$$

where λ is the maximum accepted error. For the validation procedure, it was assumed that 10% ($\lambda = 0.1$) would be the maximum accepted error for the numerical model to be considered a reasonable approximation of the real physical phenomena being modelled. From the experimental observations it can be determined that $v_f^{max} = 1700.9$ m/s and $v_f^{min} = 1447.5$ m/s. The results in Figure 3 show the numerical velocity profile for the EFP device (solid line) against the 10% error band obtained from Wu *et al.* and defined by v_f^{max} and v_f^{min} (grey band).

The numerical stable flight velocity 400 μs after detonation is 1489.6 m/s, leading to an estimated average numerical error of 7.66%. Although this error is already considered to be low, it can be further improved by optimising the model discretisation, as will be discussed below.

2.4. Element formulation and discretisation

Several convergence numerical analyses were carried out to verify the influence of the formulations, control parameters and different mesh densities. This was done based on the settings described in Sections 2.1 and 2.2, and using the experimental data provided by Wu *et al.* [25]. Numerical models

13
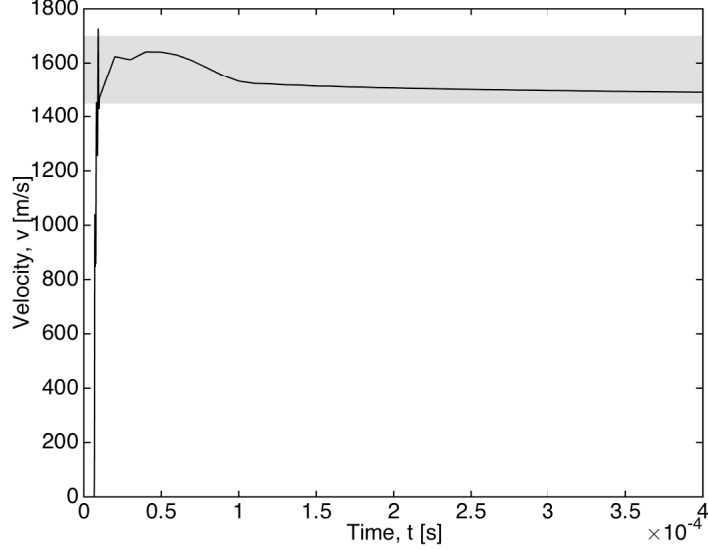
Figure 3: Numerical velocity profile for the EFP device (solid line) against the 10% error band obtained from Wu *et al.* (grey band, range defined by $v_\mathrm{f}^{\max}$ and $v_\mathrm{f}^{\min}$).

178 were discretised with 8-node hexahedral solid elements with the following

179 formulations: (i) a 1-point Eulerian formulation for the high explosive, lead-

180 ing to a discretisation that ensures good contact on the impact between the

181 shock wave and the liner/casing; and (ii) a constant stress solid element

182 Lagrangian formulation to describe the behaviour of the metallic liner.

183 Mesh refinement and optimisation was achieved based on the deforma-

184 tion histories of the liner and the explosive. A good compromise between

185 CPU time and accuracy of the numerical results was obtained by comparing

186 the stable flight velocities of the EFP with the experimental results of Wu *et*

187 *al.* [25], as described in the Model Validation section above (Section 2.3).

188 It was observed that further refining the mesh close to the liner-explosive

14

interface led to results with error levels lower than 5.5%, confirming the good predictive capability of the proposed numerical model.

The correct definition of the time step size is one important aspect on high impulsive dynamic analyses. This step size should be set to a value significantly lower than the time required for a strain wave to cross the minimum distance between two consecutive nodes ($h_{\min}$) at the wave speed in the material. Disregarding this will lead to significant computational errors and hence poor and unrealistic results. In generic terms, the critical (maximum) time step size is $\Delta t_c = h_{\min}/c$ with $c = \sqrt{E/\rho}$, where c is the wave speed, E is the elastic modulus and ρ is the density of the material. An additional 10% time step reduction is applied leading to a final maximum time step size defined by

$$\Delta t = \Delta x \sqrt{\frac{\rho h_{\min}}{100E}} \tag{6}$$

in order to minimise the possibility of occurrence of errors in the computation (*e.g.* negative volumes due to the high strain rates and pressure levels).

3. Results and discussion

The formation of an EFP is a complex dynamic process, mostly the result of the interaction between the different components of the device. The developed models were analysed in two separate stages. On the first stage the detonation of the explosive, propagation of the shock wave and

15

consequent interaction of the detonation products, accelerate and deform the liner. This stage corresponds to approximately the first 10 μs of the process. In the second stage, which corresponds to approximately 400 μs, the direct effects of the explosive, the casing and the base are neglected, and only the deformation of the projectile and its speed stabilisation are modelled.

In the context of this paper, the ballistic performance of the resulting projectile is assessed by criteria related to its kinetic energy. Ballistic parameters such as geometry, type of detonation (number and position of detonators) and materials, influence the stable flight velocity of the EFP and, consequently, its penetration ability (*i.e.* ballistic performance). Understanding the influence of each EFP design parameter on the shape and energy of the resulting projectile is thus very important and will be analysed in detail in the following sections.

3.1. Liner materials and high-explosives

The properties of the materials that constitute the EFP device are very important both in the context of the dynamic formation of the projectile and on its ballistic performance. The three-dimensional model corresponds to one quarter of the EFP, assuming two-plane symmetry. For the analyses described in this section, only one detonation point was considered, at the centre of the base of the device. All other numerical parameters are as described in Section 2. Two separate analyses were made, namely to study (i) the influence of the liner material (with dynamite as HE) and (ii) the

₂₂₂ influence of the high-explosive (with a copper liner).

₂₂₃   The results shown in Figures 4(a) and (b) show the evolution of the EFP
₂₂₄ velocity, during its formation, for different liner materials and different high-
₂₂₅ explosives, respectively. Figure 5 shows the evolution of the shape of the
₂₂₆ projectile during the early formation stages.

Figure 4: Evolution of the projectile velocity for (a) different liner materials (dynamite HE) and (b) different high-explosives (copper liner).

₂₂₇   Observed velocities exhibit a maximum during the initial stages of the
₂₂₈ formation ($0 < t < 100$ μs), which corresponds to the interaction of the
₂₂₉ detonation wave with the liner. The following stages, for $100 < t < 400$ μs,
₂₃₀ encompass most of the deformation of the liner to form the projectile and
₂₃₁ also the stabilisation of speed. Stable flight speed is reached at approxi-
₂₃₂ mately $t = 400$ μs. From the results in Figure 4(a) and Table 2 it can
₂₃₃ be observed that the copper projectile has a final speed and kinetic energy
₂₃₄ significantly higher than either iron or tantalum. The properties of copper

17
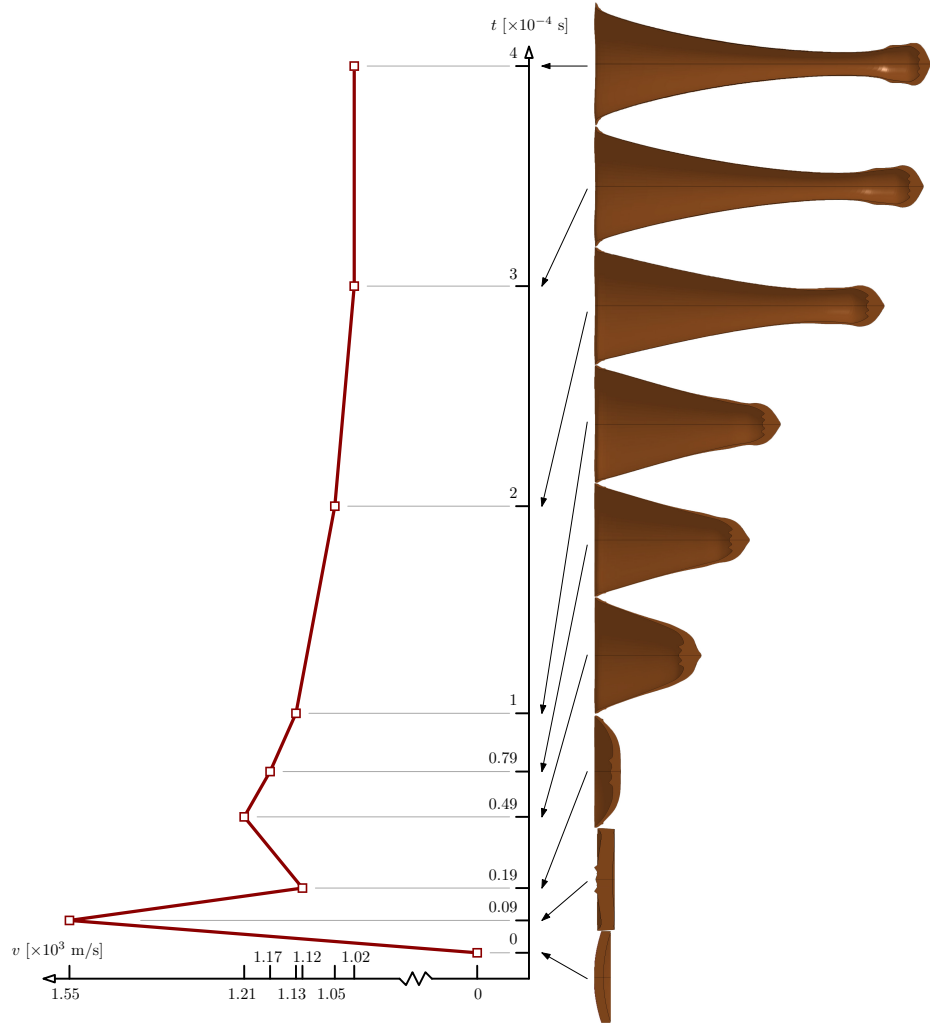
Figure 5: Evolution of the shape of the projectile during the early formation stages (for a 4 mm copper liner and dynamite HE).

²³⁵ (*e.g.* density and ductility) and its behaviour under impact, lead to the

²³⁶ conclusion that this material has optimal capacity to form an EFP with

²³⁷ high penetration capability (*i.e.* high kinetic energy).

Table 2: Stable flight velocity and resulting kinetic energy for the different material combinations.

EFP device	Projectile mass [g]	Stable flight velocity [m/s]	Kinetic energy [kJ]
Tantalum/Dyanmite	166.7	496.8	20.6
Iron/Dynamite	78.8	949.5	35.5
Copper/Dynamite	89.2	1021.8	46.6
Copper/Octol	89.2	887.5	35.1
Copper/CompB	89.2	730.1	23.8

²³⁸ Analysing the results in Figure 4(b) and Table 2, it is found that, among

²³⁹ all high-explosives tested, dynamite has the most evident effect on the final

²⁴⁰ configuration of the projectile. The speed of the explosion products and

²⁴¹ the energetic capability of the HE are responsible for this. In terms of

²⁴² final kinetic energy, copper and dynamite seem to be the most efficient

²⁴³ combination.

²⁴⁴ Copper projectiles also have a lower drag when compared to the iron

²⁴⁵ or tantalum projectiles. Although not an area of study in this work, EFP

²⁴⁶ aerodynamics are known to benefit from this type of geometry, as well as

²⁴⁷ from the formation of fins [16].

²⁴⁸ *3.2. Liner configuration*

²⁴⁹ The relation between the shape of the liner and the final geometry and

²⁵⁰ configuration of the EFP is complex and not yet fully understood [3, 14, 16].

In this section, the authors present a model that attempts to correlate the final velocity of the projectile to the initial liner geometry (*e.g.* thickness and thickness distribution). Two different liner models were used for this purpose: (i) constant thickness, five models with thicknesses ranging from 1 to 20% of the liner diameter; and (ii) variable thickness, considering two different approaches: with maximum thickness at the centre or at the edge of the liner. Model details are listed in Table 3.

Copper and dynamite were used for the liner and HE, respectively. All tests were done with a single detonation point, at the centre of the base of the EFP device (see Section 2).
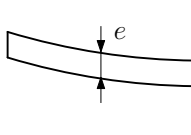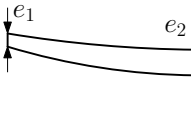
Results in Figures 6(a) and (b) show the EFP velocity during the formation stages of the projectile for the described initial liner configurations. The observed behaviour exhibits oscillations in the velocity during the initial 100 μs, corresponding to the formation of the projectile, followed by stabilisation at about $t = 200$ μs. Generically, it can also be observed that the final velocity increases with the decrease of the liner thickness. This increase is non-linear and can be approximated by the following power law:

$$v_e = k_1 e^{-\alpha} \tag{7}$$

where $k_1 = 4172$ and $\alpha = 1.048$ are constants specific for the EFP configuration and set of materials used. e is the thickness of the liner and v the final (stable flight) velocity of the EFP.

As a consequence of its curved shape, the centre of the liner receives the

20

Table 3: Stable flight velocity and resulting kinetic energy for the different liner thicknesses.

	Thickness	Liner mass [g]	Stable flight velocity [m/s]	Kinetic energy [kJ]
	$e = 2$ mm	44.6	1958.1	85.5
	$e = 4$ mm	89.2	1021.8	46.6
	$e = 5$ mm	111.5	789.8	34.8
	$e = 7$ mm	156.1	524.9	21.5
	$e = 10$ mm	223.1	369.9	15.3
	$e_1 = 2$ mm $e_2 = 4$ mm	66.1	1151.3	43.8
	$e_1 = 4$ mm $e_2 = 2$ mm	65.5	1766.0	102.1
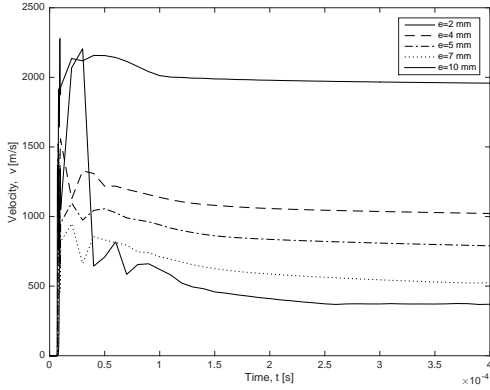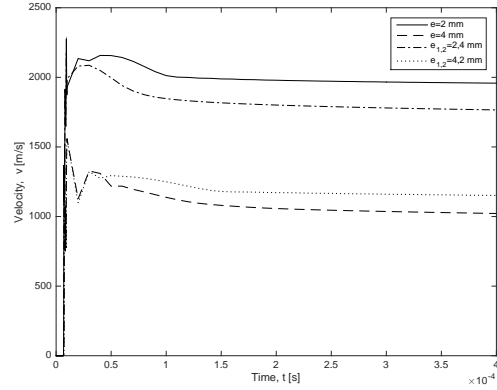
Figure 6: (a) Velocity profiles for liners with constant thickness and (b) comparison with variable thickness liners.

impact of the detonation wave before its periphery. The energy transferred to the liner accelerates and deforms it to form the projectile. When comparing variable and constant thickness models (with similar mass), there

21

seems to be a correlation between the thickness at the centre of the liner and the final EFP velocity. It was observed that the thickness at the centre of the liner is one of the most important parameters defining its final shape. Additionally, liners with a smaller centre thickness lead to higher speeds for similar masses, as can be seen from the results shown in Table 3. From the results shown in Figure 6(b) it can be observed that it is possible to change the stable flight kinetic energy just by changing the thickness (and consequently volume of material) at the periphery of the liner. Generically, from the observed results, higher stable flight velocities are obtained for liners with thicknesses between 4 and 7% of the diameter.

3.3. Layout of detonators

The number and position of the detonation points understandably has a strong influence on the whole process of releasing energy and, consequently, on the formation of the EFP, and will thus be assessed in this section. Five different sets of tests are done, with the parameters listed in Table 4 and shown in Figure 7. A complete three-dimensional FEA approach was used for the models with no symmetries. Dynamite and copper were used as HE and liner material, respectively. The liner thickness is $e = 4$ mm and the control parameters described in Section 2 were used. A synchronous detonation was assumed for all multi-detonator tests.

This study allows for a better understanding of the development of shock waves and how these influence the formation of the projectile. The EFP velocity for the various detonation parameters is shown in Figures 8(a) to (c).

22
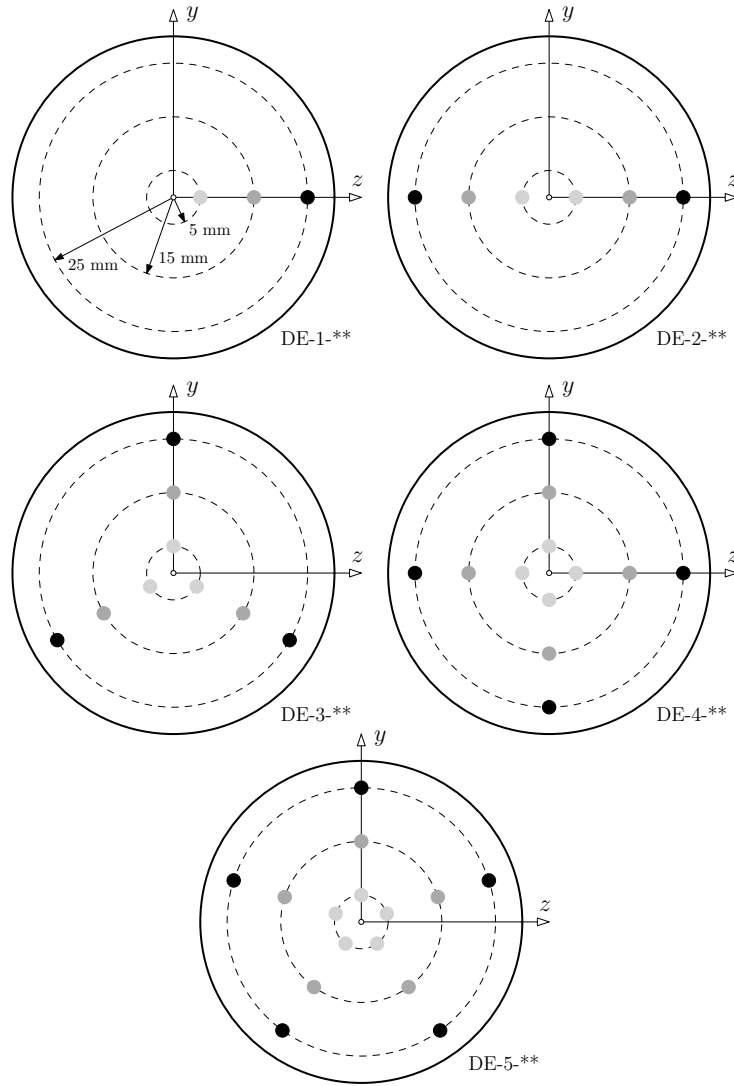
Figure 7: Number, relative position of detonators and test nomenclature (see also Table 4).

Table 4: Number and position of detonators.

Model designation	Number of detonators	Off-centre distance [mm]	Angular spacing [°]
DE-1-05		5	
DE-1-15	1	15	—
DE-1-25		25	
DE-2-05		5	
DE-2-15	2	15	180
DE-2-25		25	
DE-3-05		5	
DE-3-15	3	15	120
DE-3-25		25	
DE-4-05		5	
DE-4-15	4	15	90
DE-4-25		25	
DE-5-05		5	
DE-5-15	5	15	72
DE-5-25		25	

It can be seen from these results that the stable velocity of the EFP increases with the number of detonators. A similar effect can be observed for increasing detonator off-centre distances.

From the results in Figure 8(a), corresponding to a detonator off-centre distance of 5 mm, it can be observed that three detonation points lead to a higher stable flight velocity, as compared to the four detonation points device. From Figures 8(b) and (c), which corresponds to a detonator off-centre distance of 15 mm and 25 mm, respectively, this effect is no longer visible.

The lateral velocity of the EFP for different positions of a single detona-
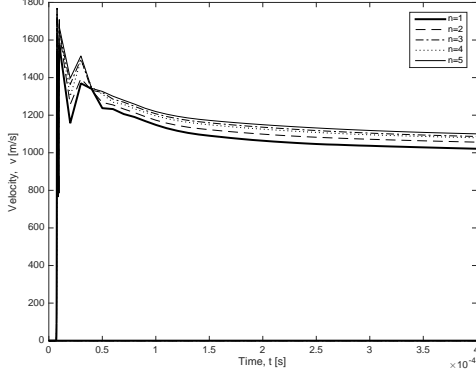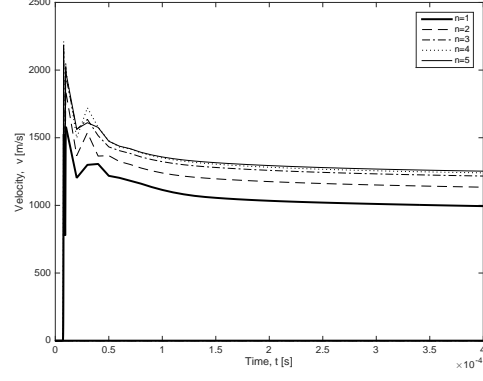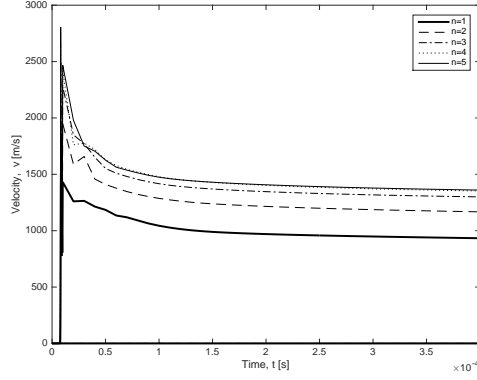
Figure 8: EFP velocity profiles with multiple detonators at off-centre distances of (a) 5 mm, (b) 15 mm and (c) 25 mm.

tor (see Figure 9) increases, as expected, with the off-centre distance. For off-centre distances larger that 15 mm the EFP becomes more unstable in flight due to the fluctuations in the lateral speed, as increasing the lateral velocity leads to a decrease on the relative axial velocity, leading to a reduction of the kinetic energy that contributes to impact and, consequently, the accuracy of the projectile. Increasing the number of detonators and

25

₃₀₇ their off-centre distance, the EFP develops more prominent fins in the final
₃₀₈ formation stages, leading to better in-flight stability and improved accu-
₃₀₉ racy [16].
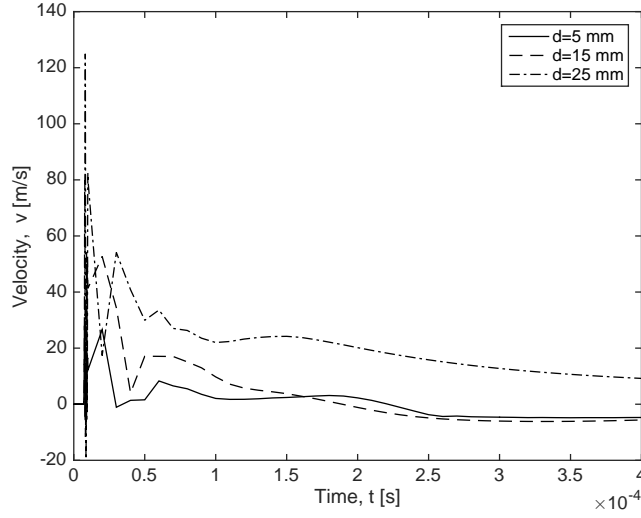
Figure 9: Lateral velocity of the EFP with one detonation point at different off-centre distances.

The power law

$$v_{\mathrm{d}} = k_2(d)n^{\gamma(d)} \tag{8}$$

describes the stable flight velocity of the EFP as a function of the number of detonators n and their off-centre distance d (see Figure 10). $k_2(d)$ and $\gamma(d)$ are linear functions of the off-centre distance of the detonators given by

$$k_2(d) = 1045 - 3.21d \tag{9}$$

26

and

$$\gamma(d) = \frac{9.9d - 1.43}{1000} \qquad (10)$$
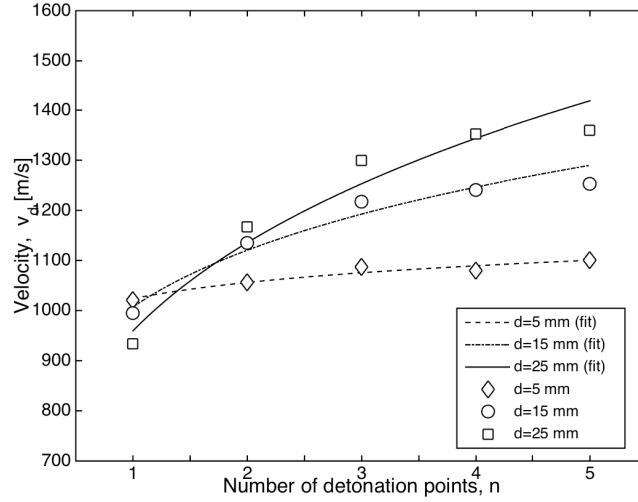
Figure 10: Stable flight velocity as a function of the number of detonators (see Equation 8).

Equations 7 and 8 can be combined to account for the influence of the thickness of the liner, yielding

$$v = v_e + (v_d - v_r) \qquad (11)$$

where v_r is a constant that accounts for the contribution of multiple detonation points. The term $(v_d - v_r)$, that represents the contribution of the type of detonation, is zero for a single central detonation point with $d = 0$, is negative for a single off-centre detonation point, and positive for multiple detonation points. Combining all previous relations, the total EFP stable

27

flight velocity is

$$v = k_1 e^{-\alpha} + k_2(d) n^{\gamma(d)} - v_{\mathrm{r}} \tag{12}$$

where $v_{\mathrm{r}} = 1024.2$ m/s for the specific device analysed in this work. An overall perspective of the relation between the projectile stable flight velocity and the configuration of the detonators (*i.e.* number and off-centre distance) is shown in Figure 11. EFP devices with different configurations (geometry, materials, HE, *etc.*) will naturally yield different curve fits and constants.
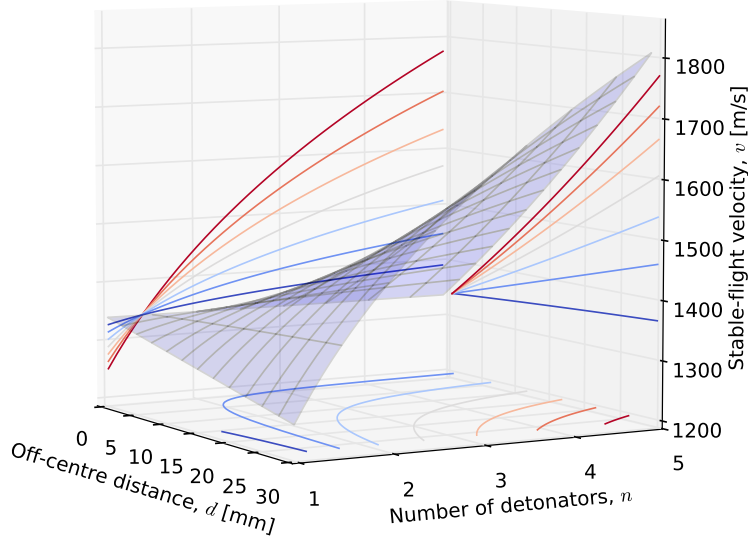
Figure 11: Stable flight velocity as a function of the number and off-centre distance of the detonators for a 3 mm constant thickness liner (see Equation 12).

3.4. EFP configuration and geometry

The configuration and dimensions of the projectile influence its behaviour both during flight and on impact. Mass should ideally be con-

centrated at the leading edge of the projectile in order to maximise focusing impact energy and thus facilitating penetration of the target. This can be better discussed by analysing the following dimensionless geometrical parameters:

$$e^* = \frac{P}{e} \qquad \text{and} \qquad \beta = \frac{L}{D} \tag{13}$$

where P, L and D are the dimensions shown in Figure 12, and e is the

thickness of the liner. Detailed results obtained for different combinations

of liner material, liner thickness, and high-explosive are listed in Table 5.
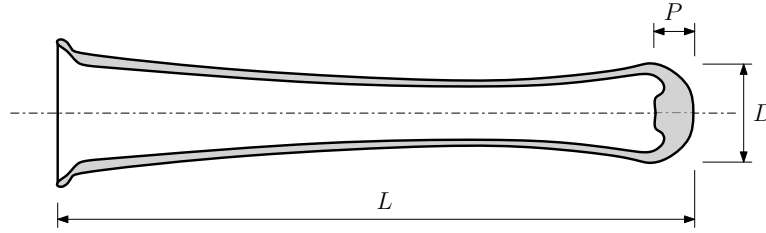
Figure 12: Transverse section of an EFP with the geometric variables used for the non-dimensional analysis.

From the analysis of different liner materials, copper is the only material

where $e^* > 1$, meaning that the thickness at the point of impact will be

higher than the initial thickness of the liner. Additionally, copper liner

EFPs have a higher aspect ratio β, an indication of a higher relative length

L and decrease in calibre D.

The results obtained for constant thickness liners show a slight increase

on e^* with increasing liner thickness, as opposed to β, which decreases

significantly, as can be seen in Figure 13.

The final geometry (*e.g.* length) of the 2 mm liner device is clearly unre-

Table 5: Geometrical parameters defining the configuration of the EFP for all analyses performed.

Models	L [mm]	D [mm]	P [mm]	e^*	β
Iron/Dynamite	69.7	35.2	3.6	0.89	1.98
Tantalum/Dynamite	33.3	34.9	3.6	0.91	0.96
Copper/Dynamite	233.4	25.8	8.8	2.21	9.03
Copper/Octol	187.4	28.1	6.6	1.65	6.66
Copper/CompB	127.8	31.2	5.2	1.31	4.10
$e = 2$ mm	555.8	20.1	4.1	2.03	27.62
$e = 4$ mm	233.4	25.8	8.8	2.21	9.03
$e = 5$ mm	165.8	27.9	14.2	2.84	5.95
$e = 7$ mm	90.9	29.3	19.3	2.74	3.10
$e = 10$ mm	71.8	49.1	39.7	3.97	1.46
$e_{1,2} = 2, 4$ mm	216.2	33.6	9.7	2.43	6.43
$e_{1,2} = 4, 2$ mm	534.6	14.9	4.0	1.98	35.98
DE-1-05	239.3	25.0	9.2	2.30	9.57
DE-1-15	236.3	24.9	9.4	2.35	9.49
DE-1-25	220.1	24.3	9.0	2.25	9.05
DE-2-05	253.1	24.0	9.5	2.37	10.56
DE-2-15	291.2	19.8	11.2	2.80	14.68
DE-2-25	315.9	17.4	12.2	3.06	18.21
DE-3-05	264.6	24.2	10.3	2.57	10.96
DE-3-15	321.9	20.3	11.9	2.98	15.89
DE-3-25	367.1	16.8	13.9	3.48	21.89
DE-4-05	262.4	24.1	10.2	2.56	10.90
DE-4-15	333.2	18.5	14.2	3.55	18.04
DE-4-25	392.0	14.1	16.2	4.05	27.83
DE-5-05	269.4	24.0	10.6	2.64	11.22
DE-5-15	341.9	19.3	13.2	3.29	17.68
DE-5-25	390.3	16.5	13.6	3.40	23.69
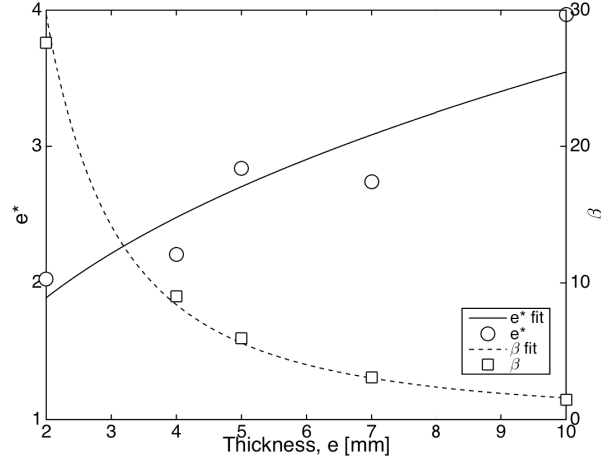
Figure 13: Dependence of e^* and β on the thickness of the liner (for constant thickness liners).

alistic. This is most probably due to the fact that the proposed model does not account for fracture/damage. By comparing the geometrical parameters to the final kinetic energy of the EFP it is possible to establish that a reasonable range for β would be $9 < \beta < 27$, corresponding to the 4 and 2 mm of constant thickness models, respectively. For the liners with variable thickness however, an exception to this interval should be made only when the kinetic energy is higher than that of the model that established the limit. By limiting β and maximising e^* it is possible to estimate the penetration capacity of the resultant EFP. From the results in Table 5 and Figure 14 it can be observed that both e^* and β gradually increase with the detonator off-centre distance, the only exception being the model with one detonation point. The model with 4 detonation points at a radial distance of 25 mm is the one with the highest values of both e^* and β. The values

31

³⁴¹ of β however, are outside the optimal interval due to the smaller calibre
³⁴² of the projectile. Therefore, the model with 5 detonation points at 25 mm
³⁴³ off-centre distance has better results within the accepted values.

³⁴⁴   As previously stated, the detonation parameters of an EFP strongly
³⁴⁵ influence the final configuration of the projectile. To illustrate this, the
³⁴⁶ view along the axis of each EFP model is shown in Figure 15, where the
³⁴⁷ effects of the detonation parameters become evident.
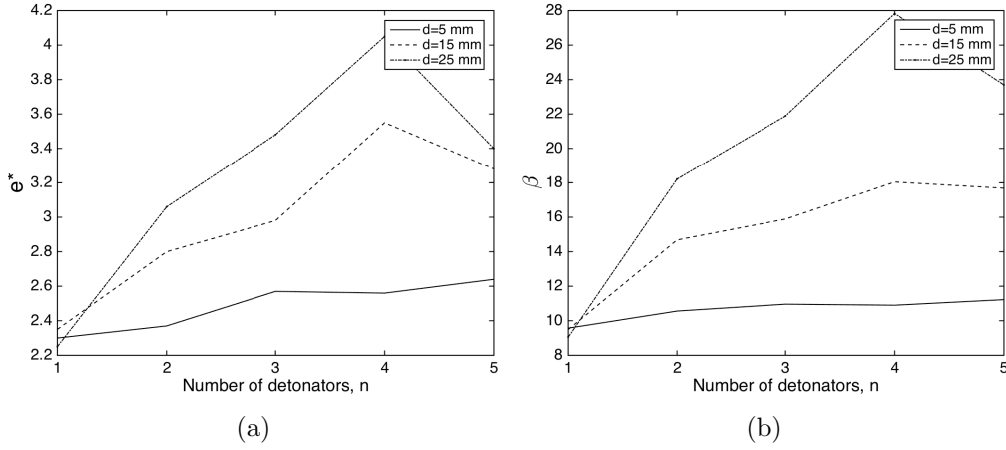
Figure 14: Relation between (a) e^* and (b) β, and the number and position of detonators, for constant thickness liners.

³⁴⁸ 4. Conclusions

³⁴⁹   In the present paper the authors propose and describe a finite element
³⁵⁰ based numerical model of a medium calibre explosively formed projectile
³⁵¹ (EFP) device. This model is based on a generic EFP with an aspect ratio
³⁵² of 1.07 and is initially validated against experimental observations. This

(a) DE-1-05   (b) DE-1-15   (c) DE-1-25   (d) DE-2-05

(e) DE-2-15   (f) DE-2-25   (g) DE-3-05   (h) DE-3-15

(i) DE-3-25   (j) DE-4-05   (k) DE-4-15

(l) DE-4-25   (m) DE-5-05   (n) DE-5-15   (o) DE-5-25
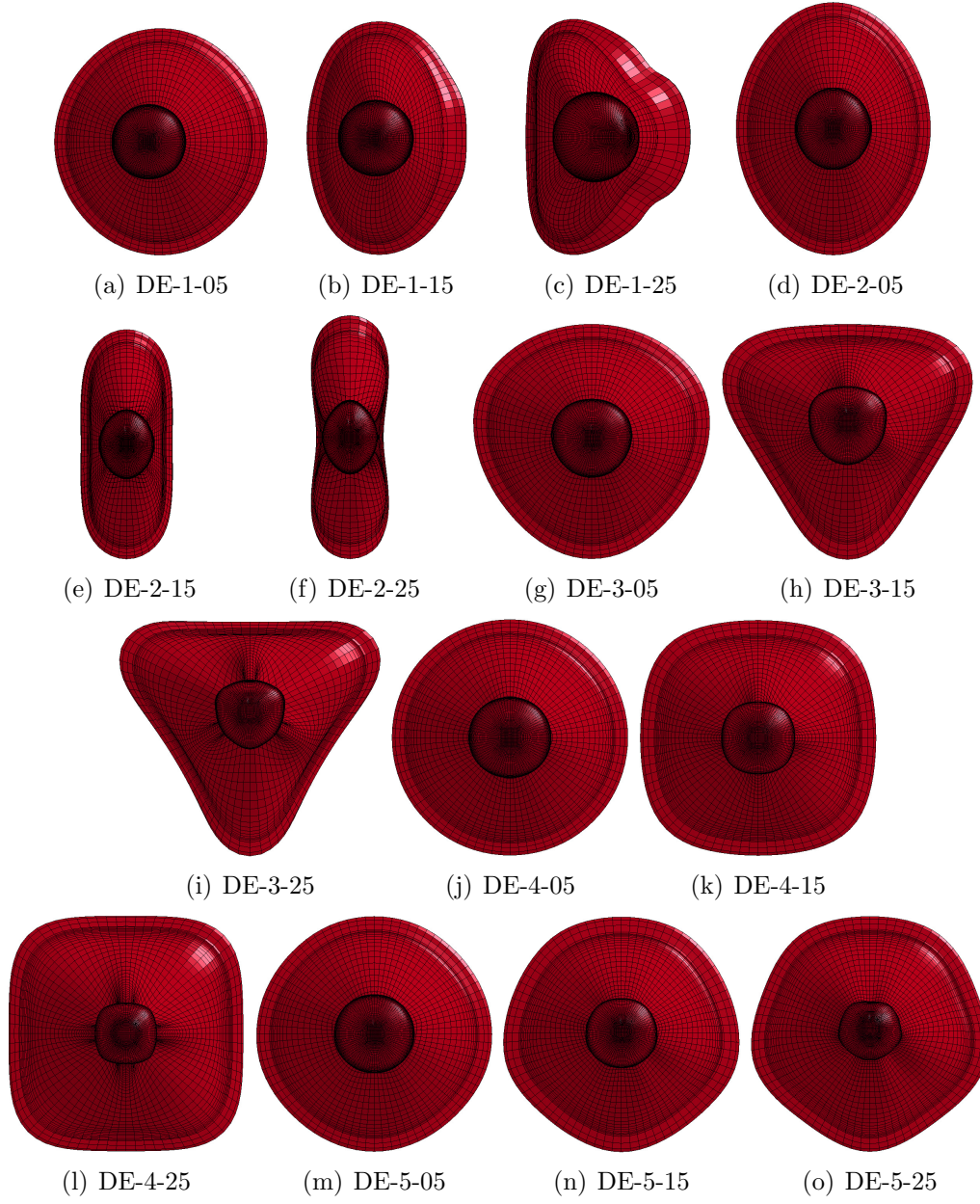
Figure 15: View along the axis of the projectiles with 1 to 5 detonation points at 5, 15 and 25 mm off-centre distance (see Table 4 for test nomenclature).

approach is then used to assess the influence of the liner materials and thickness, geometrical imperfections (*i.e.* variability in liner thickness), high-explosive, and number and off-centre distance of detonators on the performance of the projectile. This performance is quantified by analysing the formation stage of the projectile, the stable flight velocity profiles and the projectile configuration (based on a set of non-dimensional geometrical parameters).

In generically terms and from the results obtained it is shown that the thickness (and thickness variability) of the liner is one of the most important factors, along with the off-centre distance of the detonator(s), influencing the stable flight velocity of the EFP. It is also observed that, within the materials and range of parameters tested, the most performant (and aggressive) EFP has a liner with thickness between 4 and 7% of its diameter, a copper liner and dynamite high-explosive (HE). For variable thickness liners however, results show that there is a relationship between the centre thickness of the liner and the final velocity achieved, proving more advantageous to have a smaller thickness closer to the centre of the liner, resulting in higher velocities for such a mass and thus higher kinetic energy.

In evaluating geometric parameters of the EFP, more specifically the study of the effect of varying the liner thickness in the projectile, the results obtained from the performed simulations show that with increasing mass of the projectile and with the same L/D ratio of the explosive, the final speed of the projectile decreases.

In the evaluation of the effects of detonation parameters, namely the number and the distance to the centre of the explosive, there were significant improvements in the results obtained from simulations as the number of detonators increased. The same happened when their off-centre distance increased, the exception being the single point detonation. An increasing tendency for the development of fins was also observed for increasing number of detonators and off-centre distance. In terms of kinetic energy, the EFP with five detonation points with 25 mm of radial distance proved most advantageous presenting the maximum final velocity for the same projectile mass.

The numerical models developed are able to correctly predict the complex behaviour of an EFP and evaluate the influence of different materials/configurations used. An analytical model is also proposed, which can be used to predict the stable flight velocity of the EFP based on the materials, configuration and detonation parameters. This analytical model has however, some limitations, the most important being the consideration of a perfectly synchronous detonation when multiple detonators are present.

References

[1] W. Payman, D.W. Woodhead, H. Titman. Explosion waves and shock waves, Part II – The shock waves and explosion products sent out by blasting detonators. *Proceedings of Royal Society of London* **148**:604-622, 1935.

[2] R.W. Wood. Optical and physical effects of high explosives. *Proceedings of The Royal Society of London* **157A**:249-261, 1936.

[3] G.R. Johnson. Dynamic analysis of explosive-metal interaction in three dimensions. *Journal of Applied Mechanics* **48**(1):30-35, 1981.

[4] G.R. Johnson, R.A. Stryk. Some considerations for 3D EFP computations. *International Journal of Impact Engineering* **32**:1621-1634, 2006.

[5] J.A. Zukas, D.R. Scheffler. Practical aspects of numerical simulations of dynamic events: effects of meshing. *International Journal of Impact Engineering* **24**:925-945, 2000.

[6] E.A. Taylor. Simulation of hollow shaped charge jet impacts onto aluminium whipple bumpers at 11 km/s. *International Journal of Impact Engineering* **26**:773-784, 2001.

[7] U. Nyström, K. Gylltoft. Numerical studies of the combined effects of blast and fragment loading. *International Journal of Impact Engineering* **36**:995-1005, 2009.

[8] J.F. Molinari. Finite element simulation of shaped charges. *Finite Elements in Analysis and Design* **38**:921-936, 2002.

[9] S. Miller. A new design criteria for explosively-formed hypervelocity projectile (EFHP). *International Journal of Impact Engineering* **10**:403-411, 1990.

[10] R.E. Brown, M.E. Majerus, J. S. Lewis. Building characteristics into a shaped charge to achieve unique performance requirements. *International Journal of Impact Engineering* **17**:121-130, 1995.

[11] C.A. Weickert, P.J. Gallagher. Penetration of explosively formed projectiles. *International Journal of Impact Engineering* **14**:809-818, 1993.

[12] Y. Chuan, T. Yanjin, Y. Chengli, L. Fabo, G. Yulin, Z. Ming, W. Bingren, X. Panhai, L. Liangzong. Applied research of shaped charge technology. *International Journal of Impact Engineering* **23**:981-988, 1990.

[13] D. Bender, J. Carleone. *Tactical Missile Warheads*, in: Progress in Astronautics and Aeronautics, American Institute of Aeronautics and Astronautics, Vol. 155, 1993.

[14] K. Weimann, K. Doenngsfeld. *Modeling, testing, and analysis of EFP performance as a function of confinement.* in: Proceedings of the 12th International Symposium on Ballistics, 228-237, 1990.

36

[15] C.A. Weickert, P.J. Gallagher *Ogive-nosed, finned, explosively-formed projectiles,* in: Proceedings of the 16th International Symposium on Ballistics, 613-614, 1996.

[16] D. Bender, J. Carleone. *Method and apparatus for providing a explosively formed penetrator having fins.* United States Patent, num. 5365852, Nov. 22, 1994.

[17] S. Pappu, L.E. Murr. Hydrocode and microstructural analysis of explosively formed penetrators. *Journal of Materials Science* **37**:233-248, 2002.

[18] G.R. Johnson, W. Cook. *A constitutive model and data for metal subjected to large strains, high strain rates and high temperatures.* in: Proceedings of the 7th International Symposium on Ballistics, 541-547, 1983.

[19] G. Johnson, W. Cook. Fracture characteristics of three metals subjected to various strains, strain rates, temperatures and pressures. *Engineering Fracture mechanics* **21**(1):31-48, 1985.

[20] F. Zerilli, R. Armstrong. Dislocation mechanics based constitutive relations for material dynamics calculations. *Journal of Applied Physics* **61**:1816-1825, 1987.

[21] J.R. Assay, G.I. Kerley. The response of materials to dynamic loading. *International Journal of Impact Engineering* **5**:69-99, 1987.

[22] S.M. Cardonne, P. Kumar, C.A. Michaluk, H.D. Schwartz. Tantalum and its alloys. *International Journal of Refractory Metals and Hard Materials* **13**:187-194, 1995.

[23] M. Katayama, S. Kibe, T. Yamamoto. Numerical and experimental study on the shaped charge for space debris assessment. *Acta Astronautica* **48**:363-372, 2001.

[24] L.E. Murr, M.A. Meyers, C.S. Niou, Y.J. Chen, S. Pappu, C. Kennedy. Shock-induced deformation twinning in tantalum. *Acta Materialia* **45**:157-175, 1997.

[25] J. Wu, J. Liu, Y. Du. Experimental and numerical study on the flight and penetration properties of explosively-formed projectile. *International Journal of Impact Engineering* **34**:1147-1162, 2007.

[26] W. Li, X. Wang, W. Li. The effect of annular multi-point initiation on the formation and penetration of an explosively formed penetrator. *International Journal of Impact Engineering* **37**:414-424, 2010.

37

[27] A.H. Cordesman, M. Allison, J. Lemieux. *IED Metrics for Afghanistan January 2004 — September 2010.* Center for Strategic & International Studies, November 11, 2010.

[28] C. Whitlock. *Number of U.S. casualties from roadside bombs in Afghanistan skyrocketed from 2009 to 2010.* The Washington Post, January 25, 2011.

[29] M. Jean-Louis, W. Fetterhoff, M. Hadar. *Faces of the fallen.* The Washington Post. Retrieved from http://apps.washingtonpost.com/national/fallen/, April, 2015.

[30] G.A. Christou, L.R. Young, R. Goel, A.P. Vechart, A. Jerusalem. Shock attenuation of PMMA sandwich panels filled with soda-lime glass beads: A fluid-structure interaction continuum model simulation. *International Journal of Impact Engineering,* **47**:48-59, 2012.

[31] K. Vahedi, N. Khazraiyan. *Numerical modeling of ballistic penetration of long rods into ceramic/metal armors*, in: 8$^{\text{th}}$ International LS-Dyna Users Conference: Drop/Impact simulations **14**:39-50, 2004.

[32] C.E. Zhou, G.R. Liu, K.Y. Lou. Three-dimensional penetration simulation using smoothed particle hydrodynamics. *International Journal of Computational Methods* **4**:671-691, 2007.

[33] J. Hallquist. *LS-Dyna Theory Manual.* Livermore Software Technology Corporation, March 2006.

[34] M.L. Wilkins. Calculations of Elastic Plastic Flow. *Methods in Computational Physics* **3**:211-263, 1964.

[35] E.D. Giroux. *HEMP User's Manual.* Lawrence Livermore National Laboratory, University of California, Rept. UCRL-51079, 1973.

[36] P.A. Urtiew, B. Hayeo. Parametric study of the dynamic JWL-EOS for detonation products. *Fizika Goreniya i Vzryva,* **27**(4):126-137, 1991.

38

Casing · High-explosive · Liner

$\alpha/2$

R

d · D

e

e'

L

Oxz plane
symmetry

z

x

y

Oxy plane
symmetry

On-axis detonation point

High-explosive   Casing   Liner
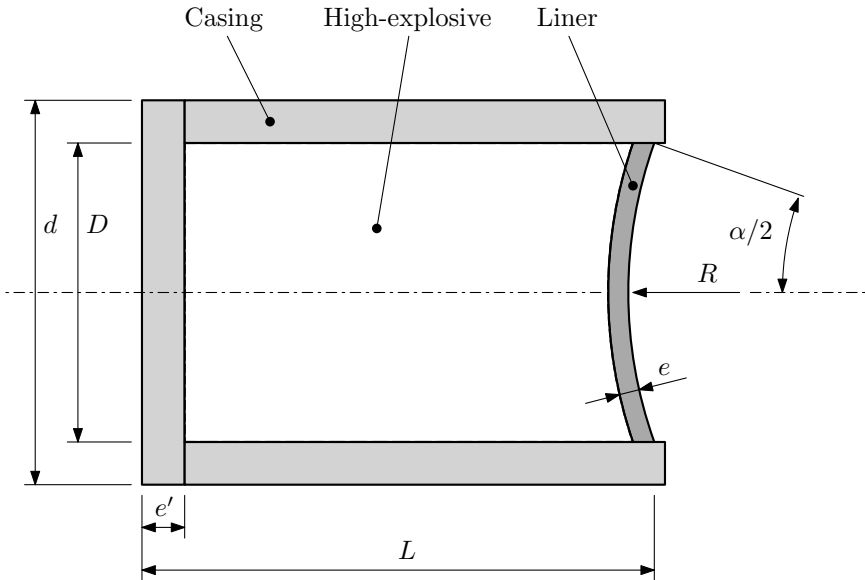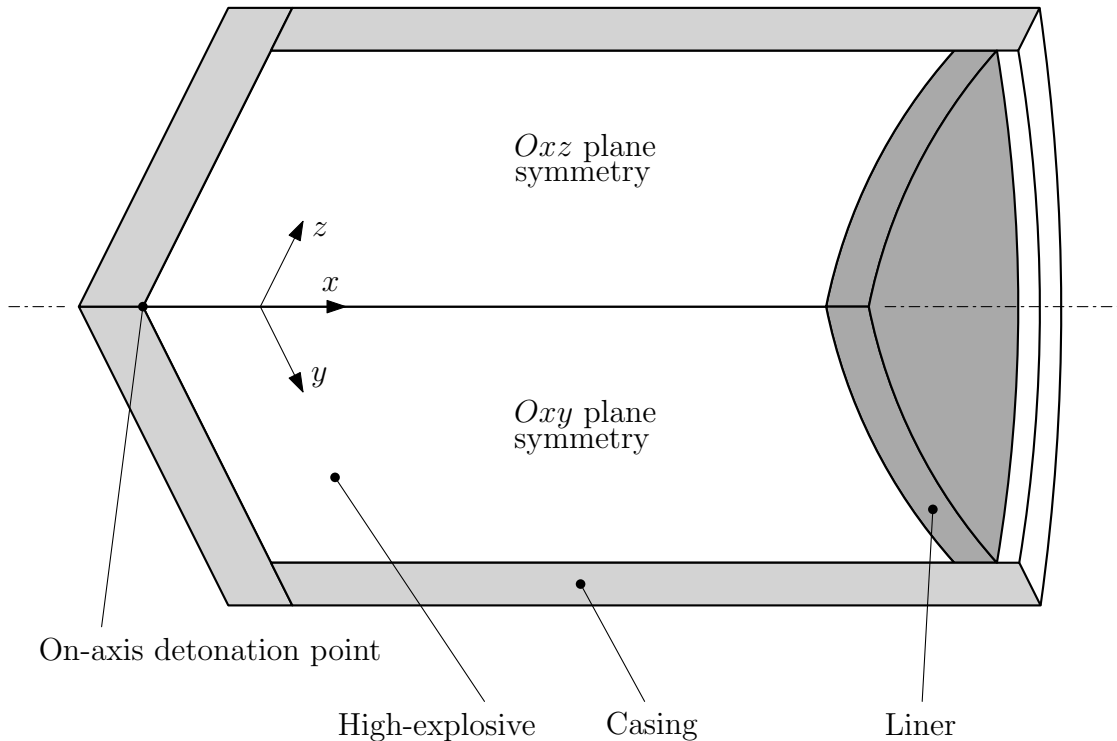
Figure 3

Figure 4a

Figure 4b

$t\ [\times 10^{-4}\ \mathrm{s}]$

4

3

2

1

0.79

0.49

0.19

0.09

0

$v\ [\times 10^{3}\ \mathrm{m/s}]$

1.55   1.21   1.17   1.13   1.12   1.05   1.02   0

Figure 6a

Figure 6b

DE-1-**

DE-2-**

DE-3-**

DE-4-**

DE-5-**

5 mm

15 mm

25 mm
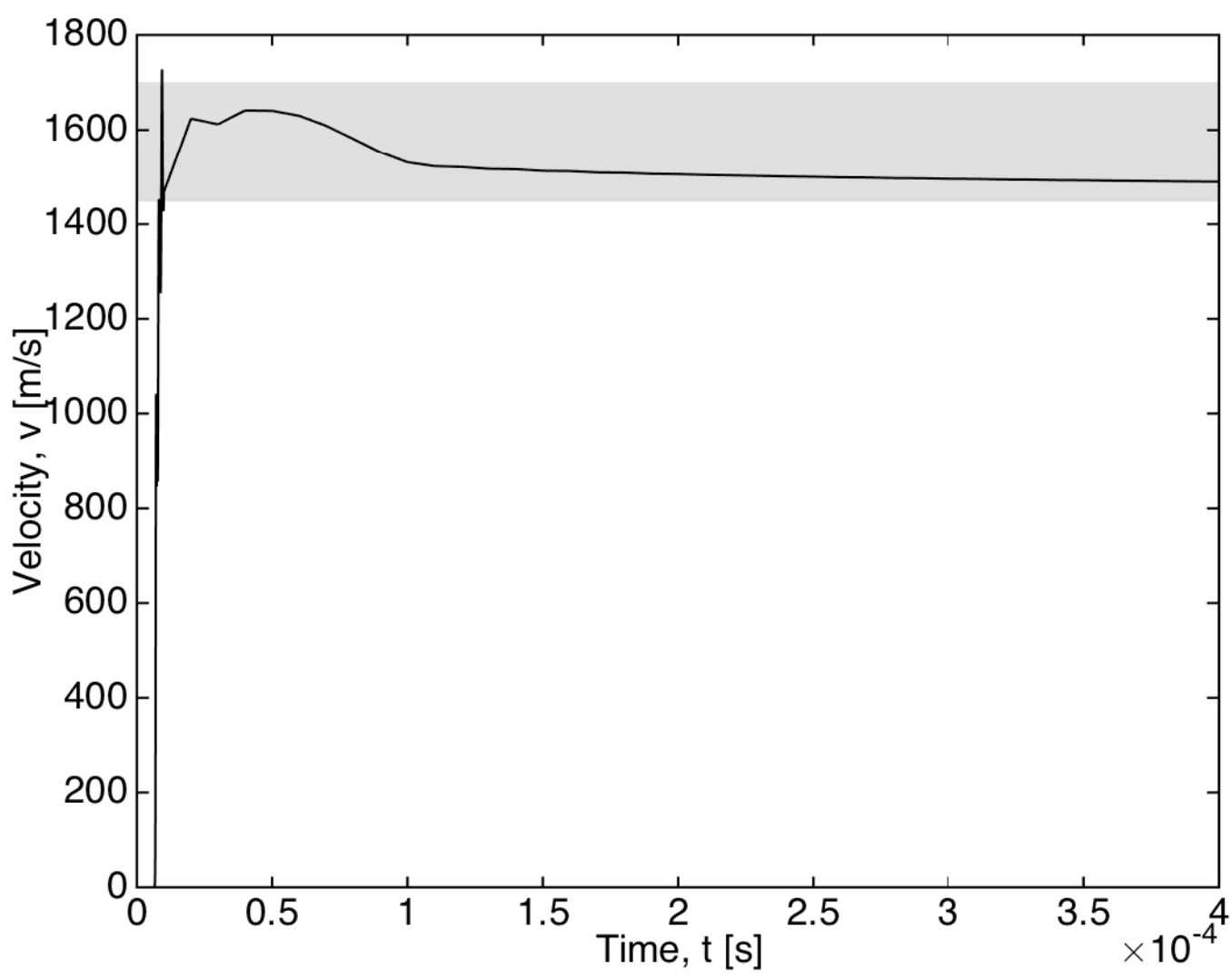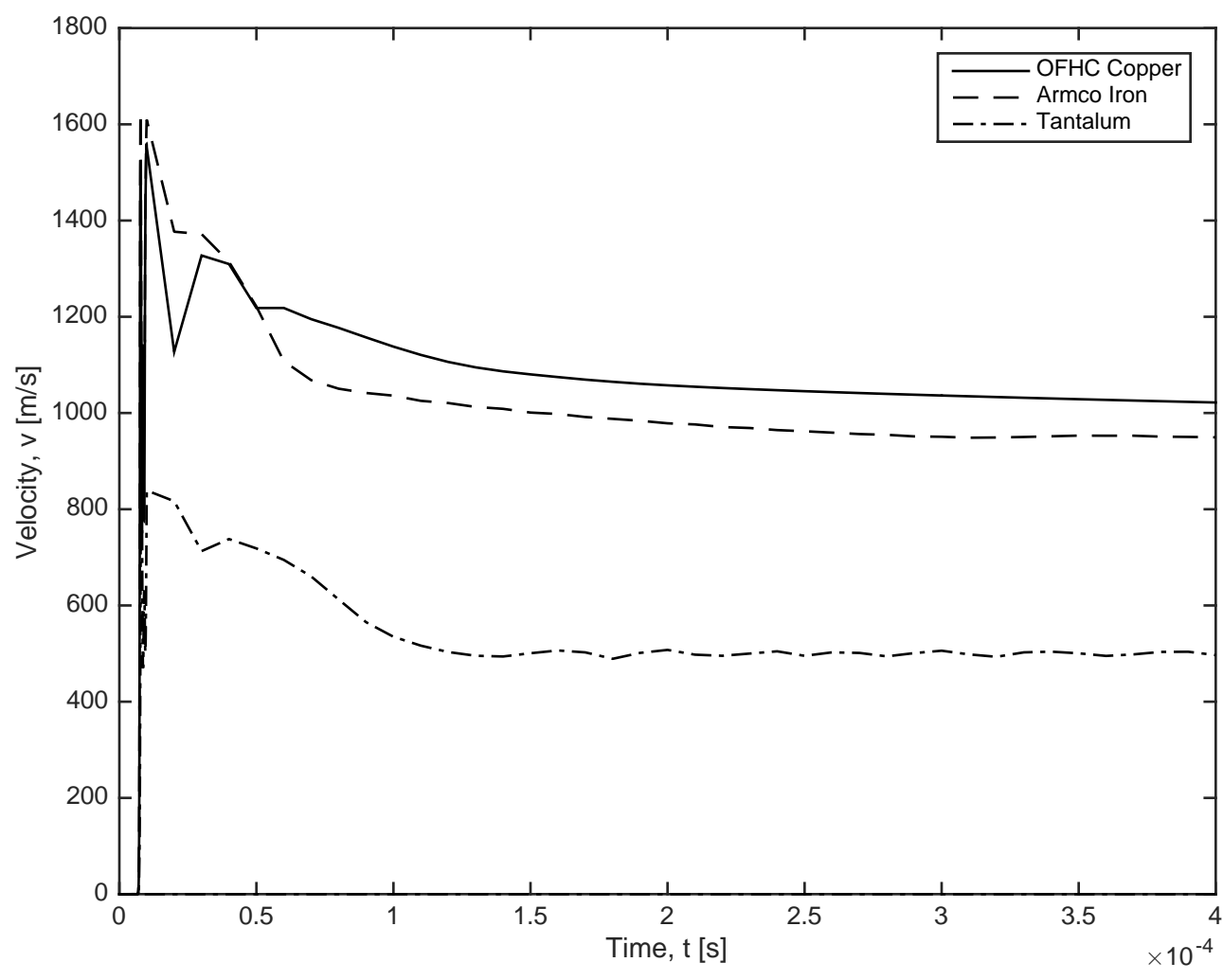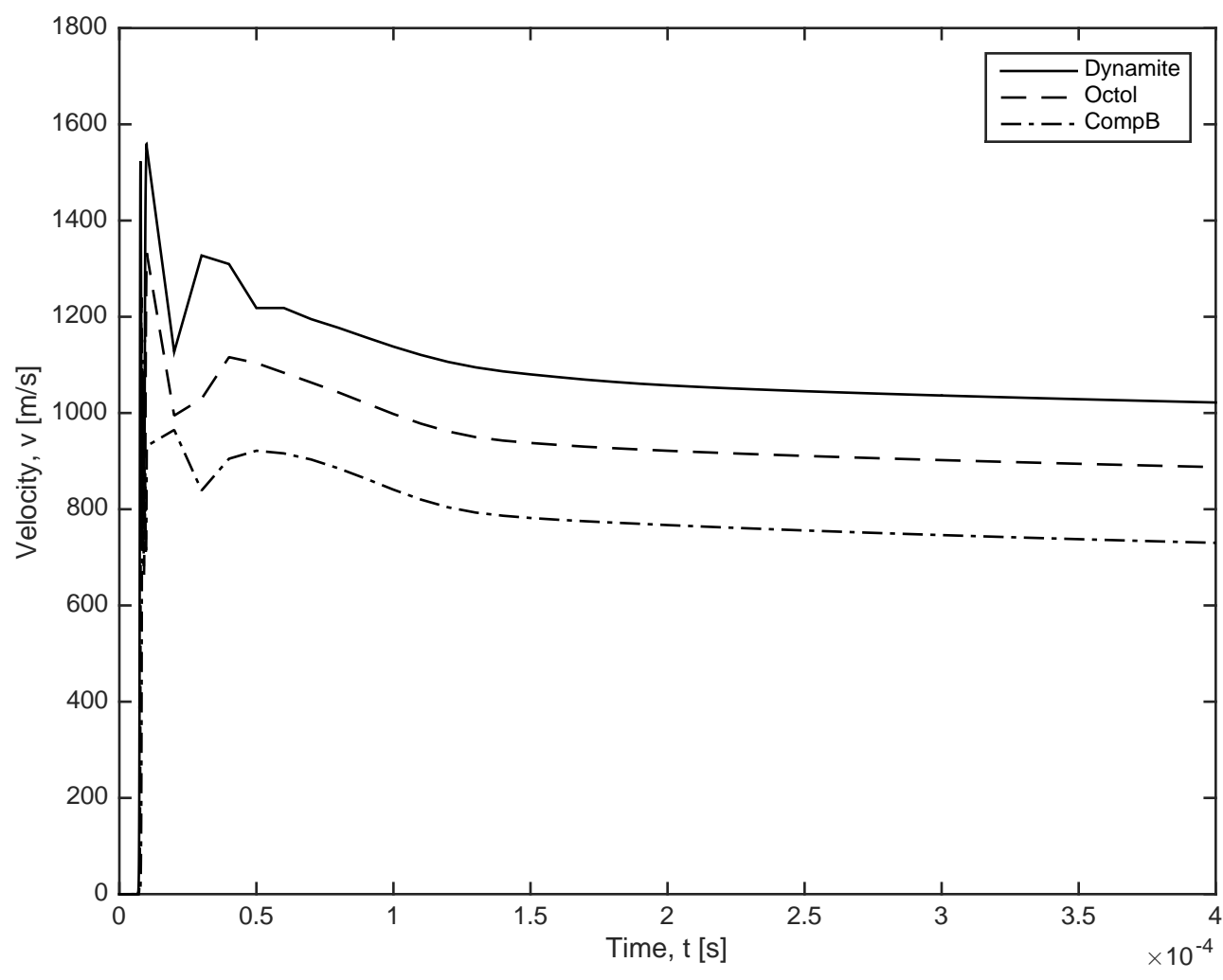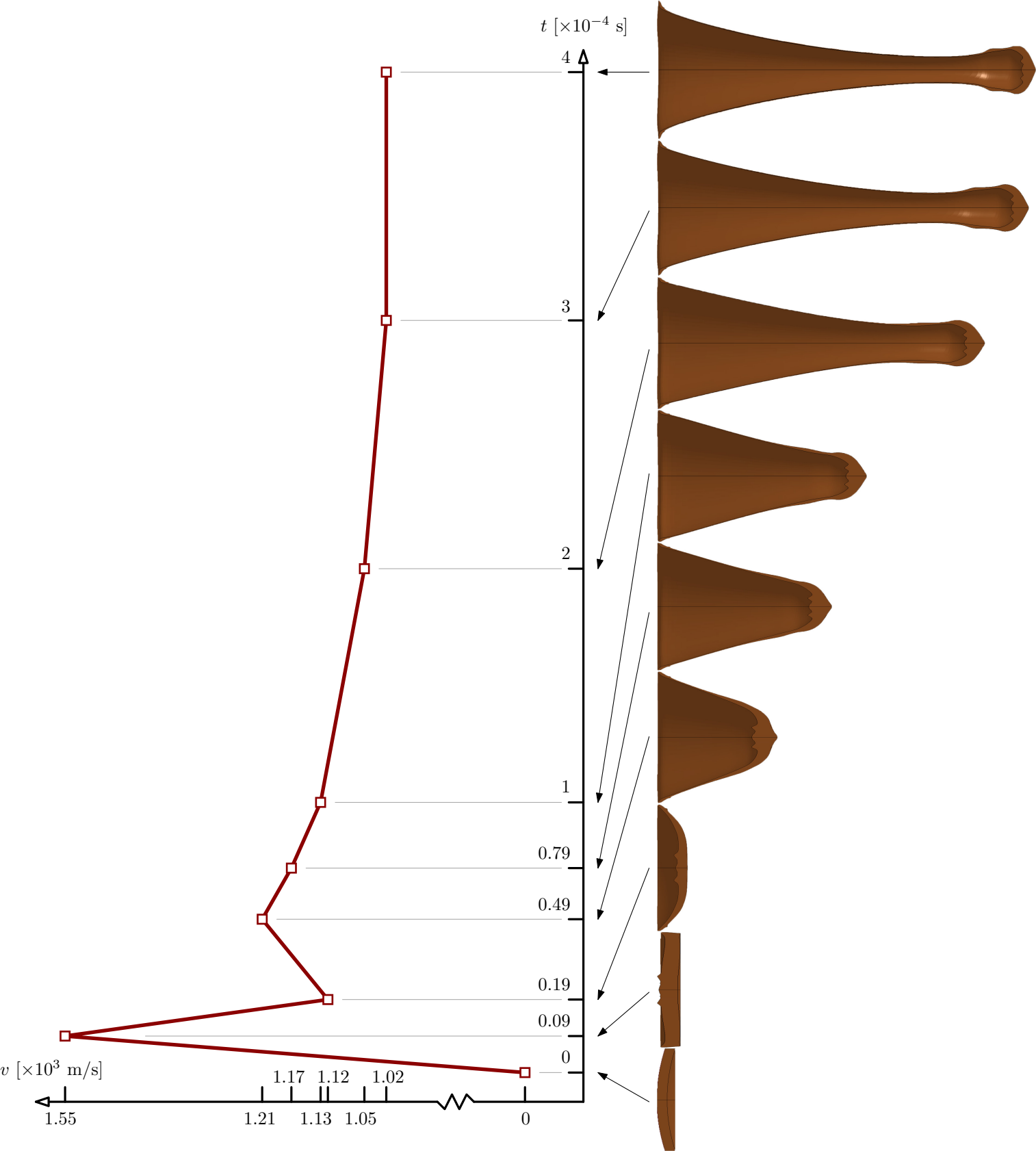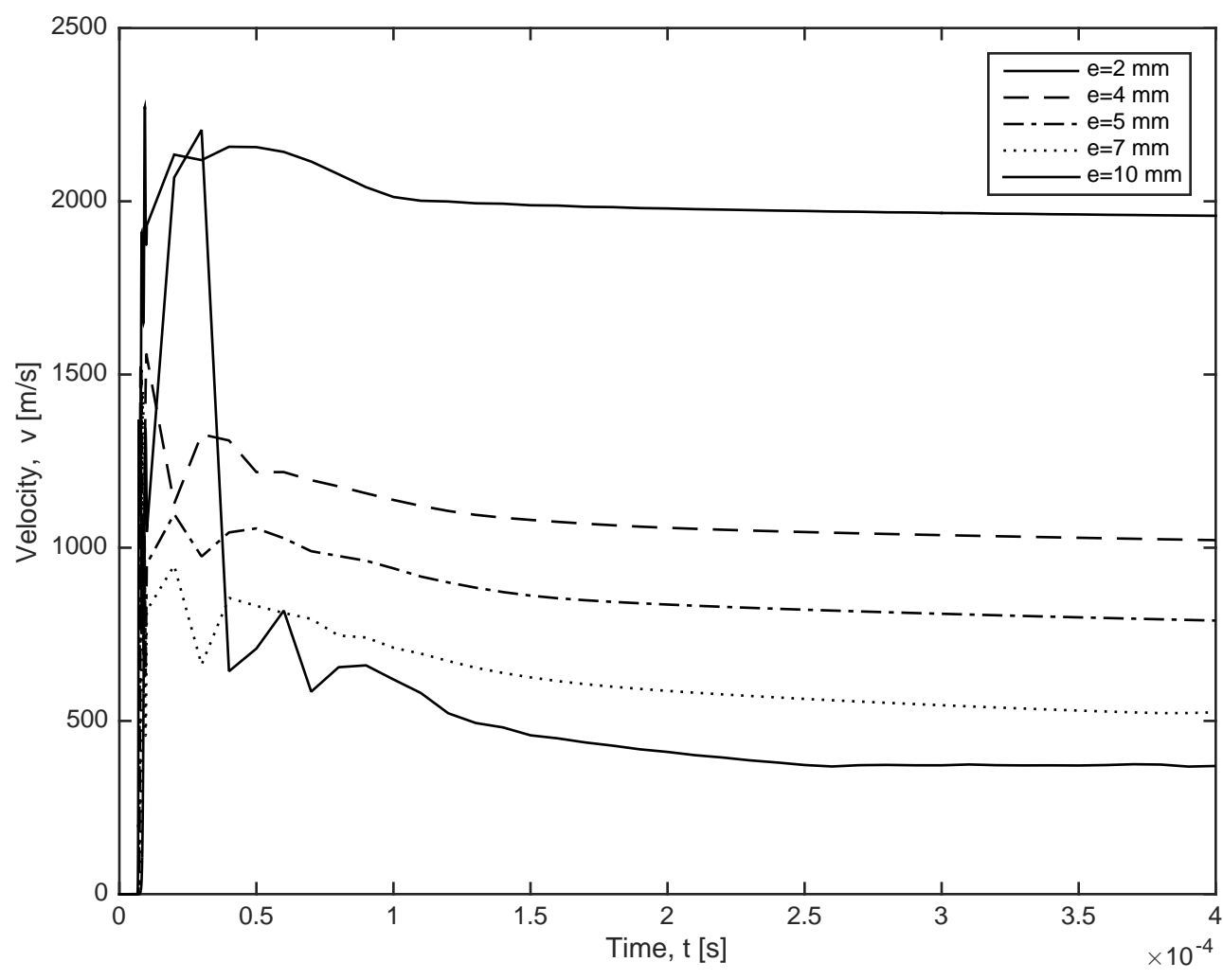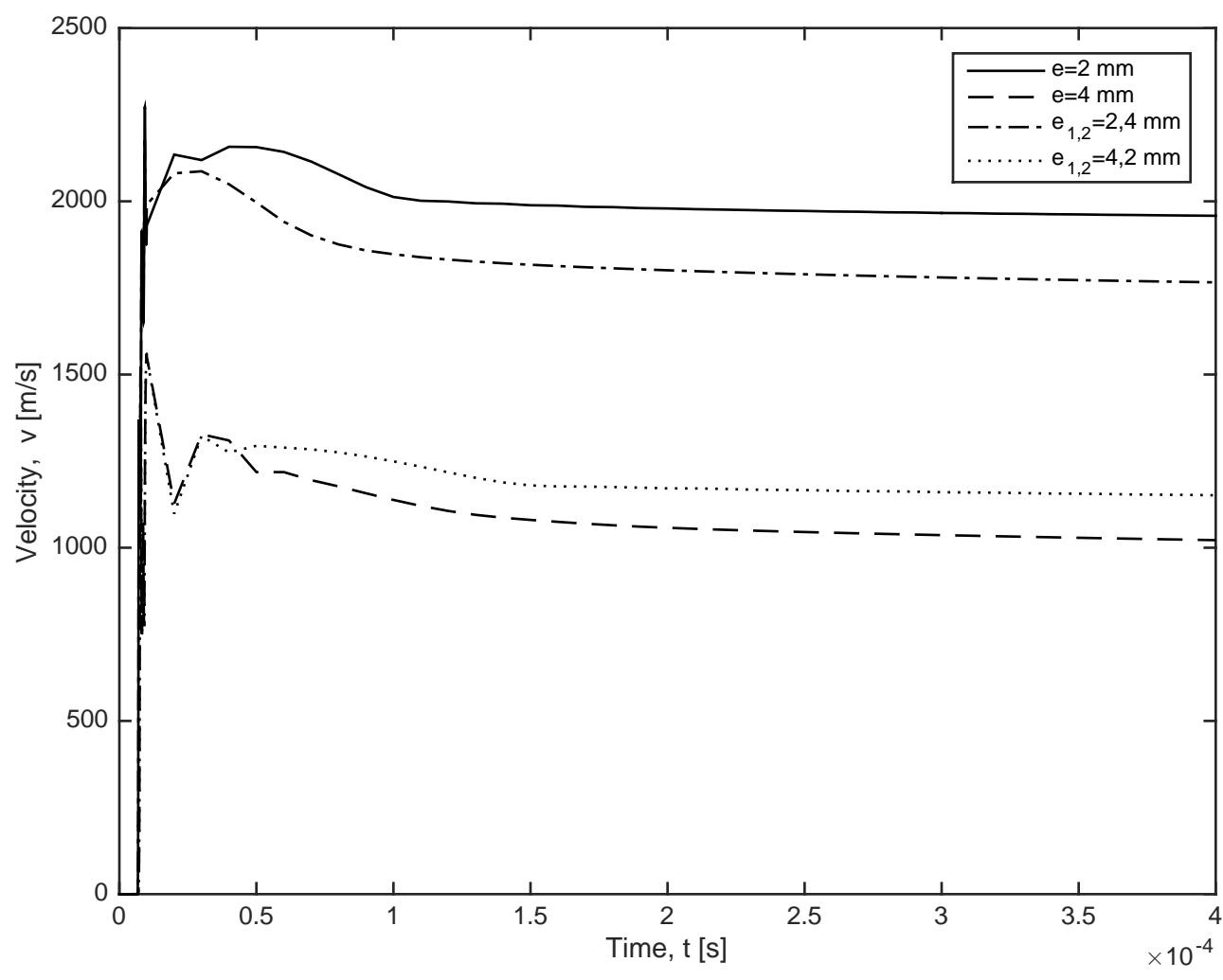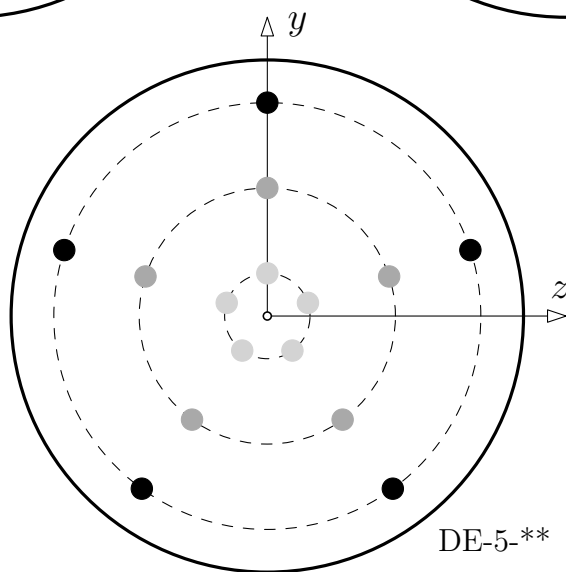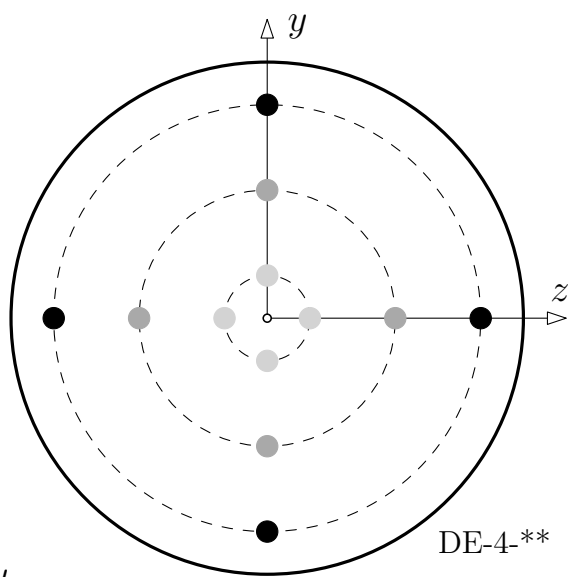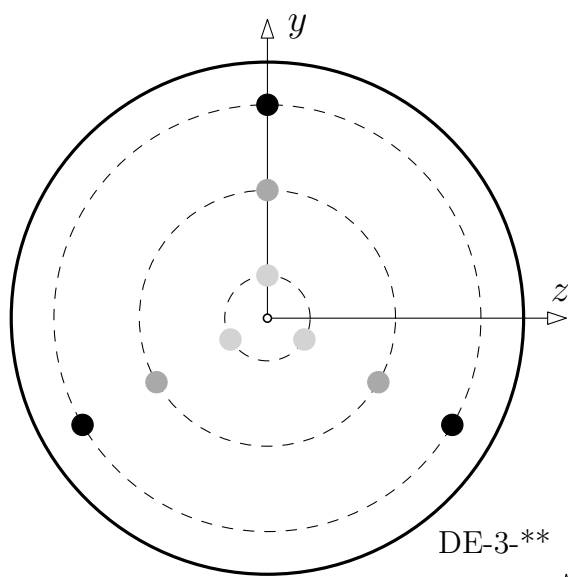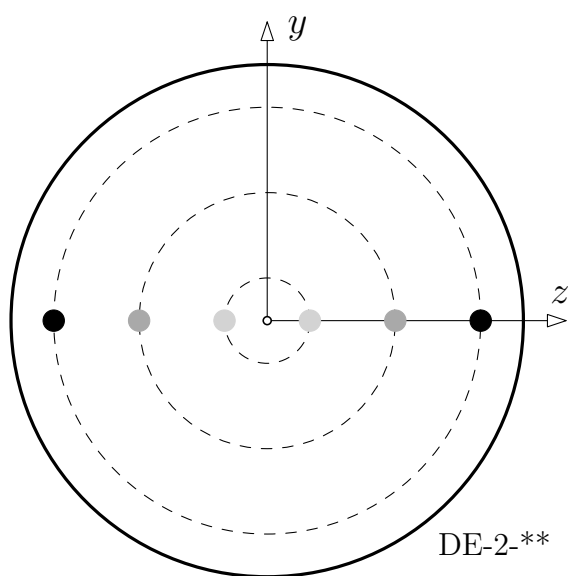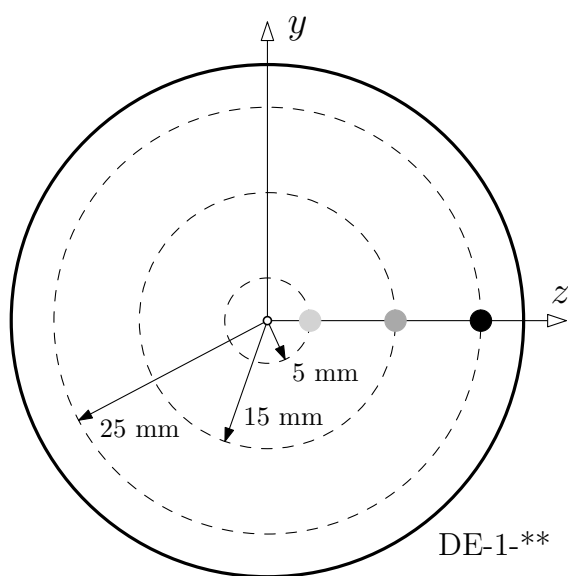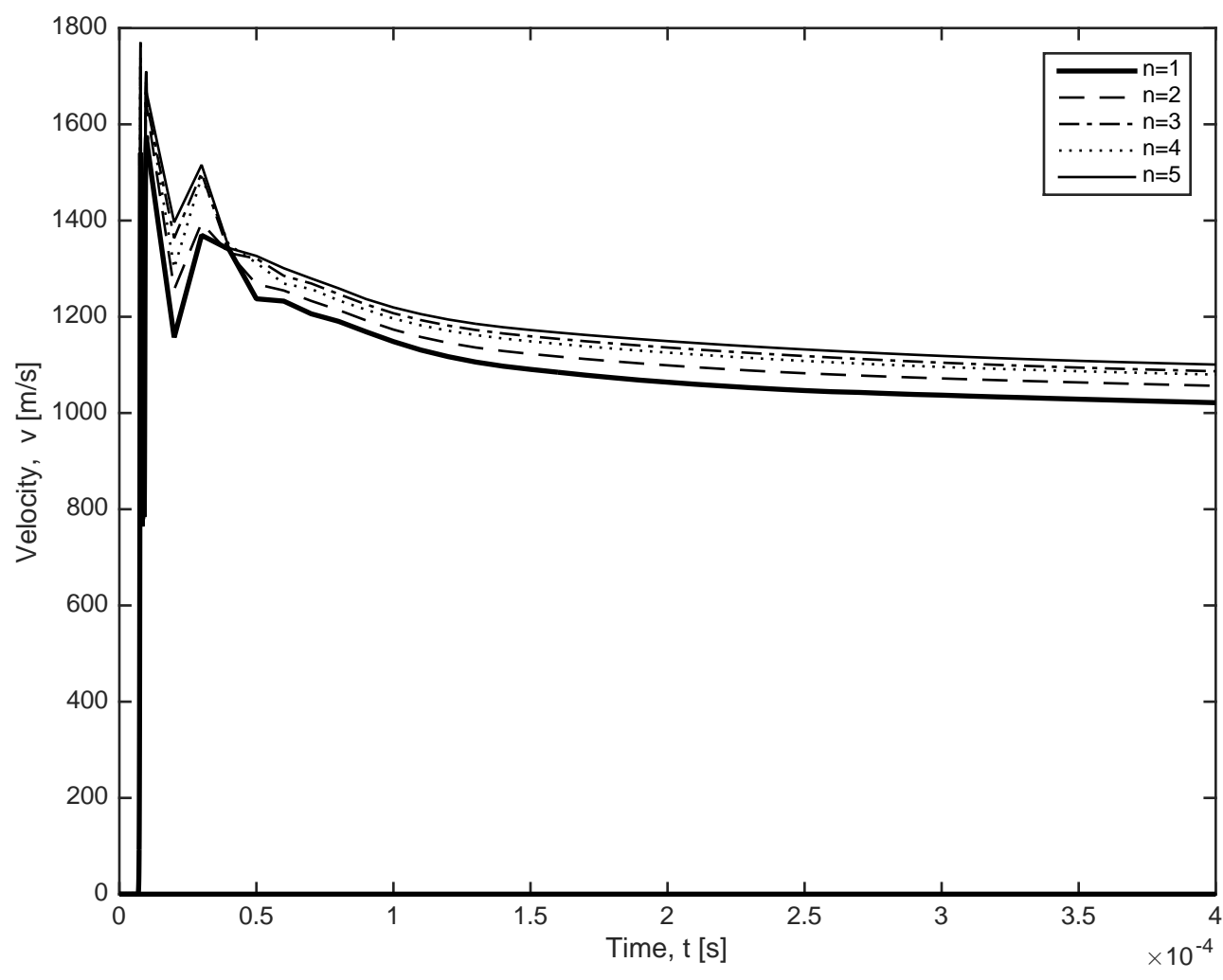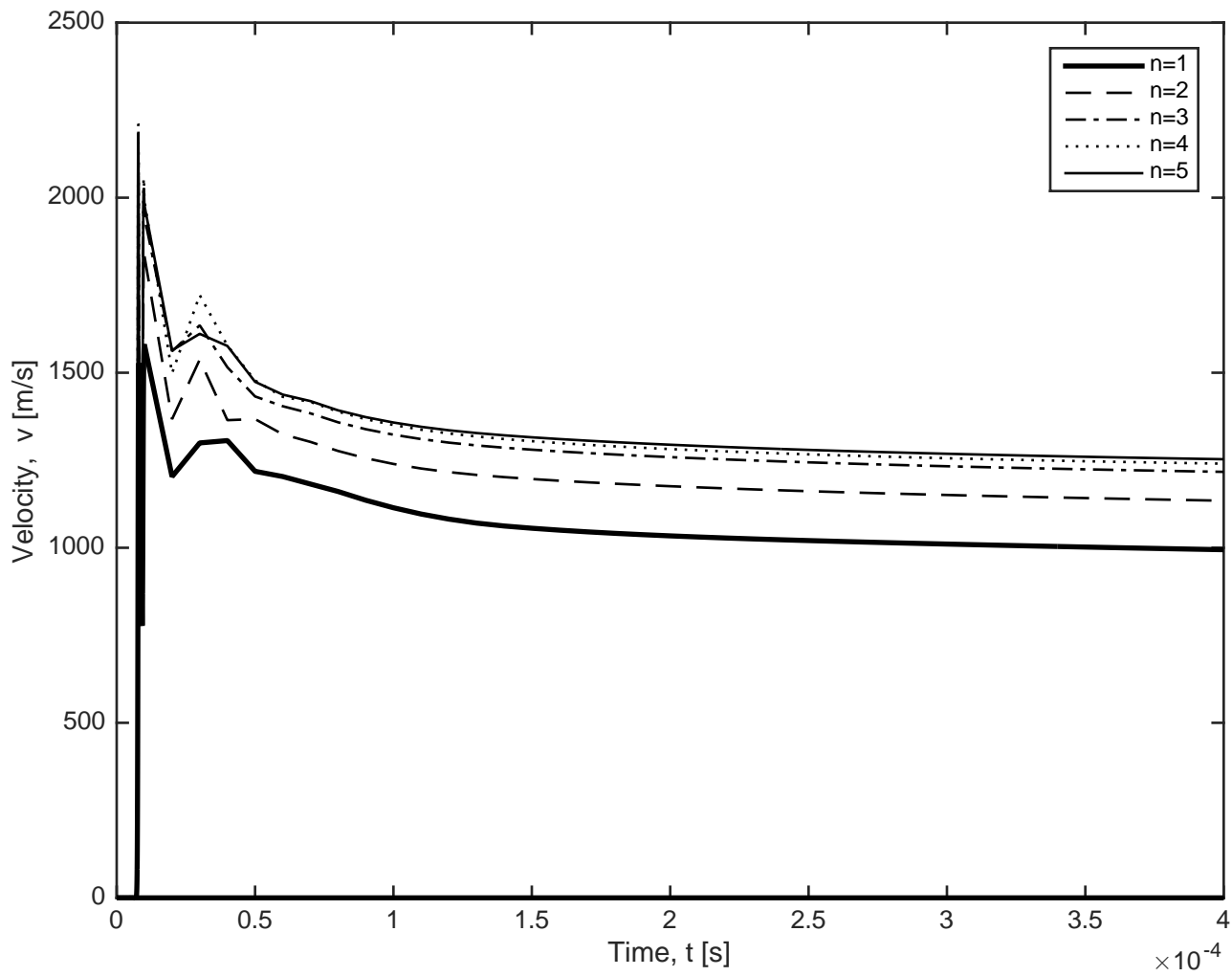
Figure 8a

Figure 8b

Figure 8c
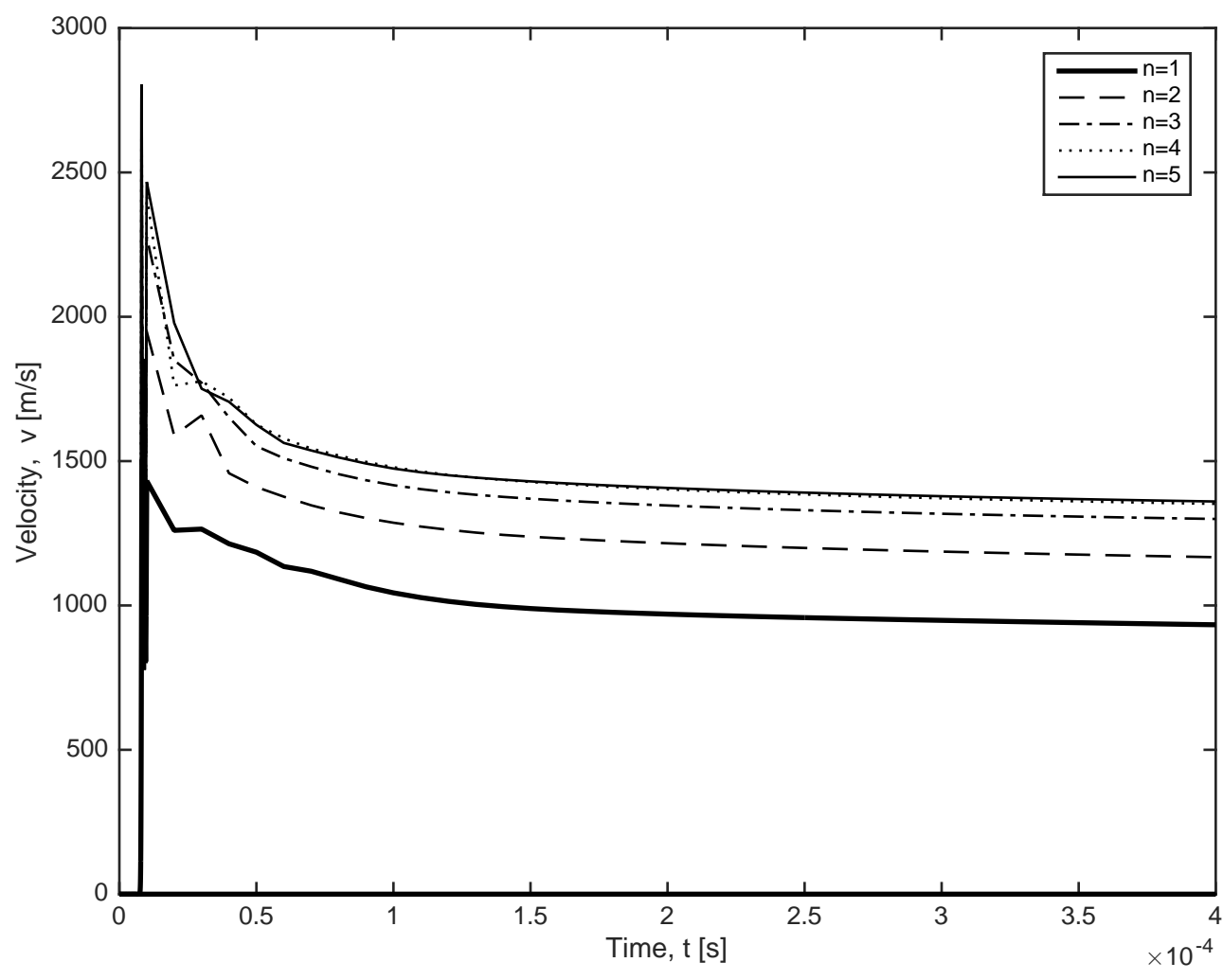
Figure 9
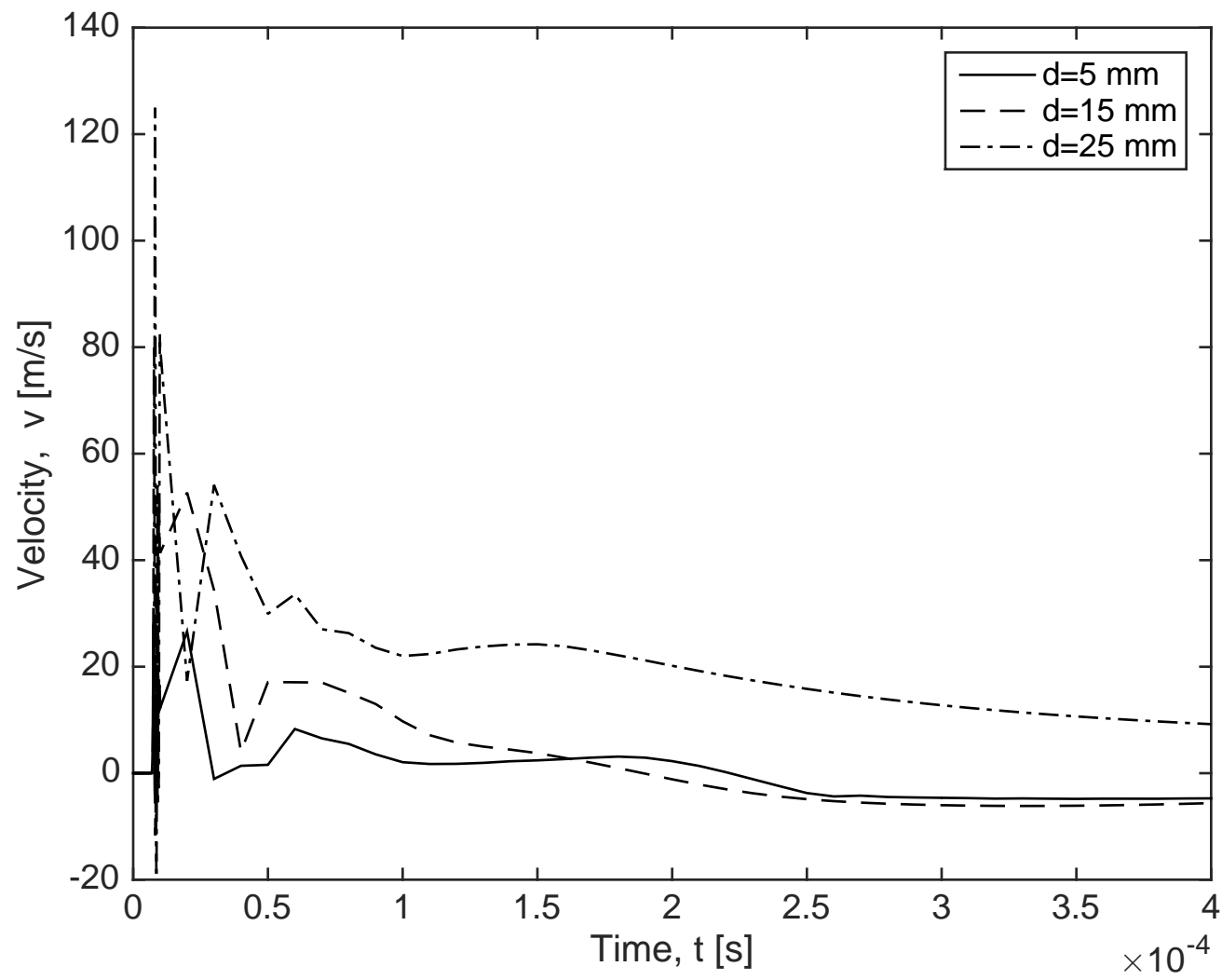
Figure 10
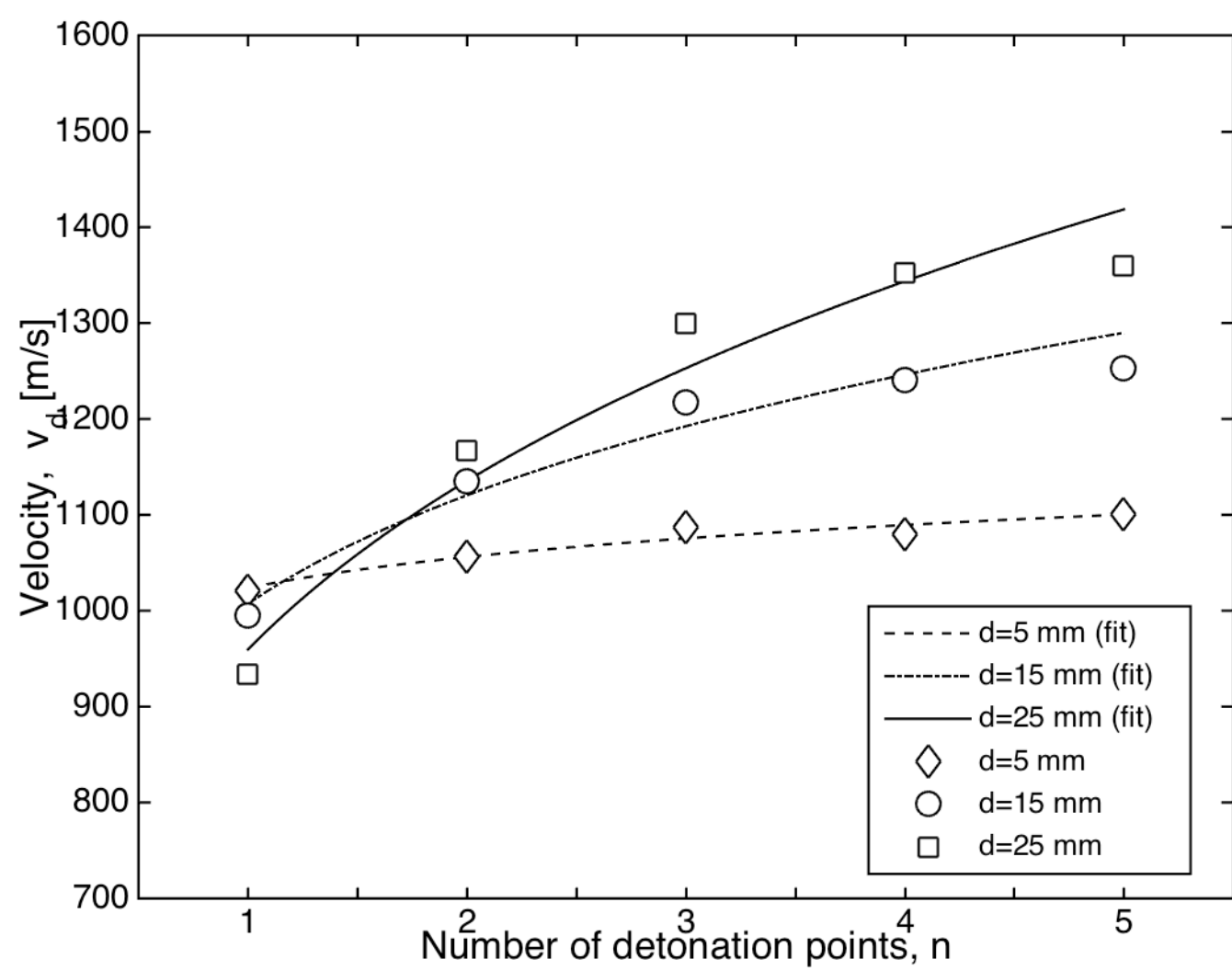
Figure 11
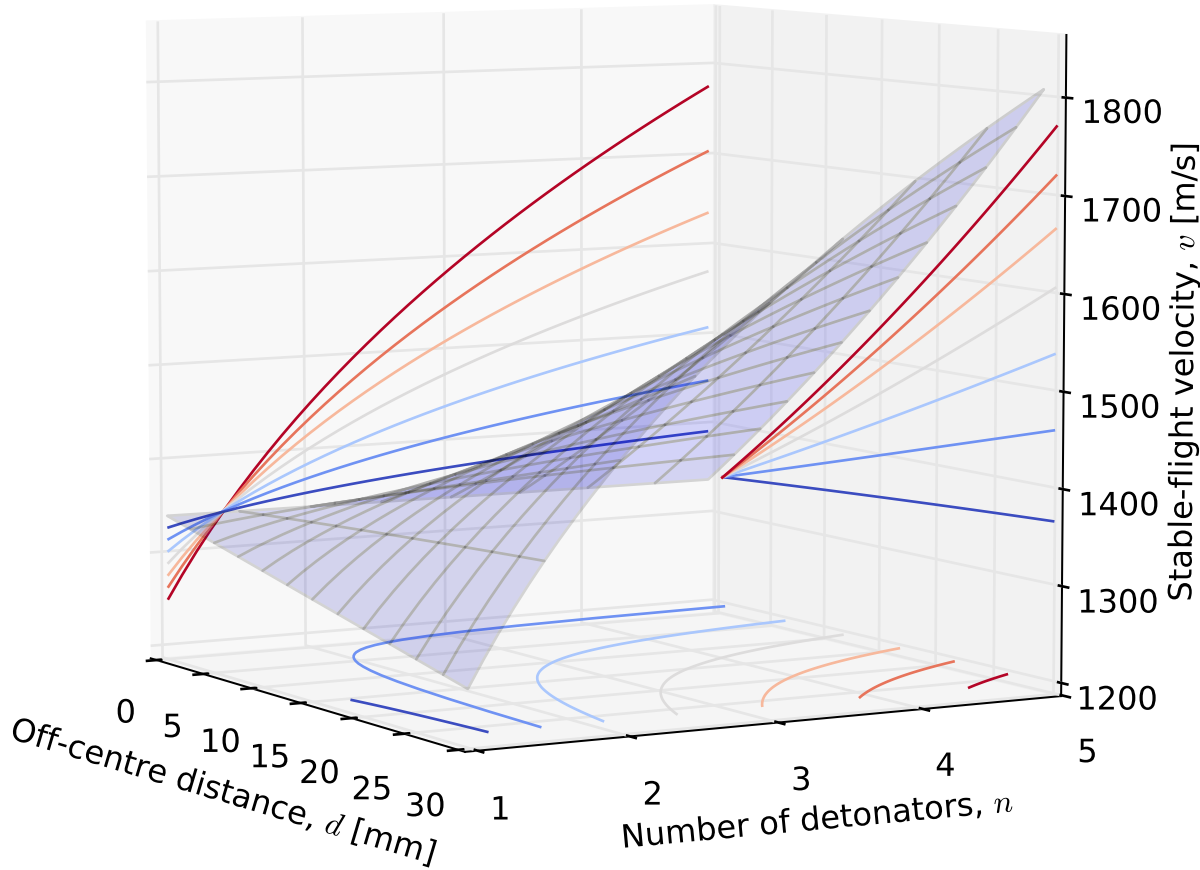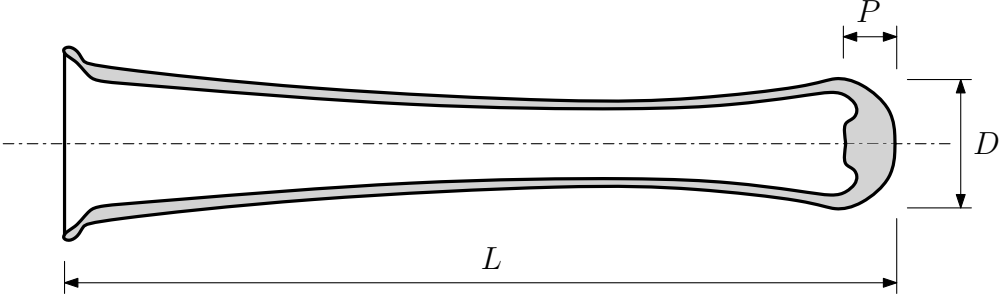
Figure 13
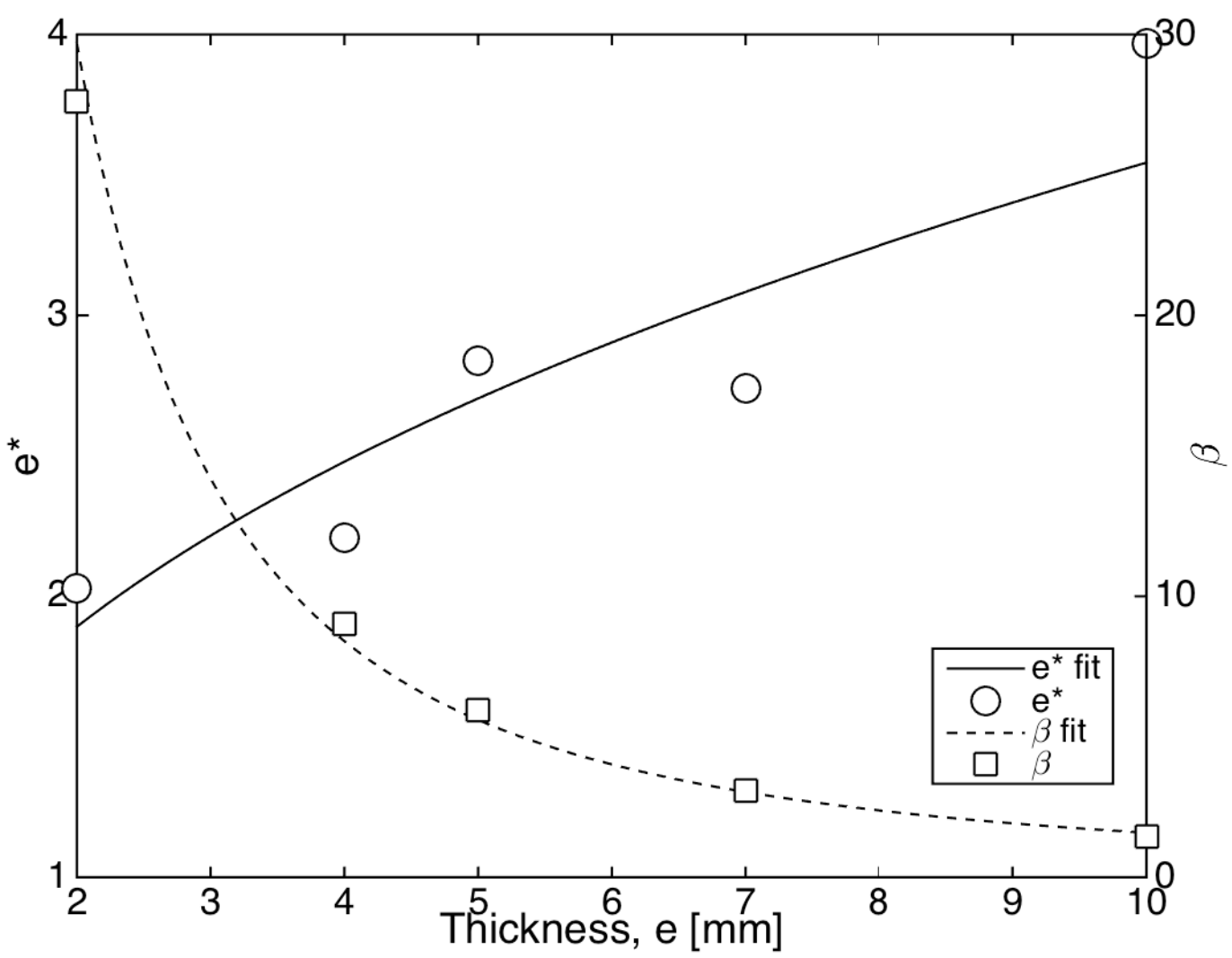
Figure 14a
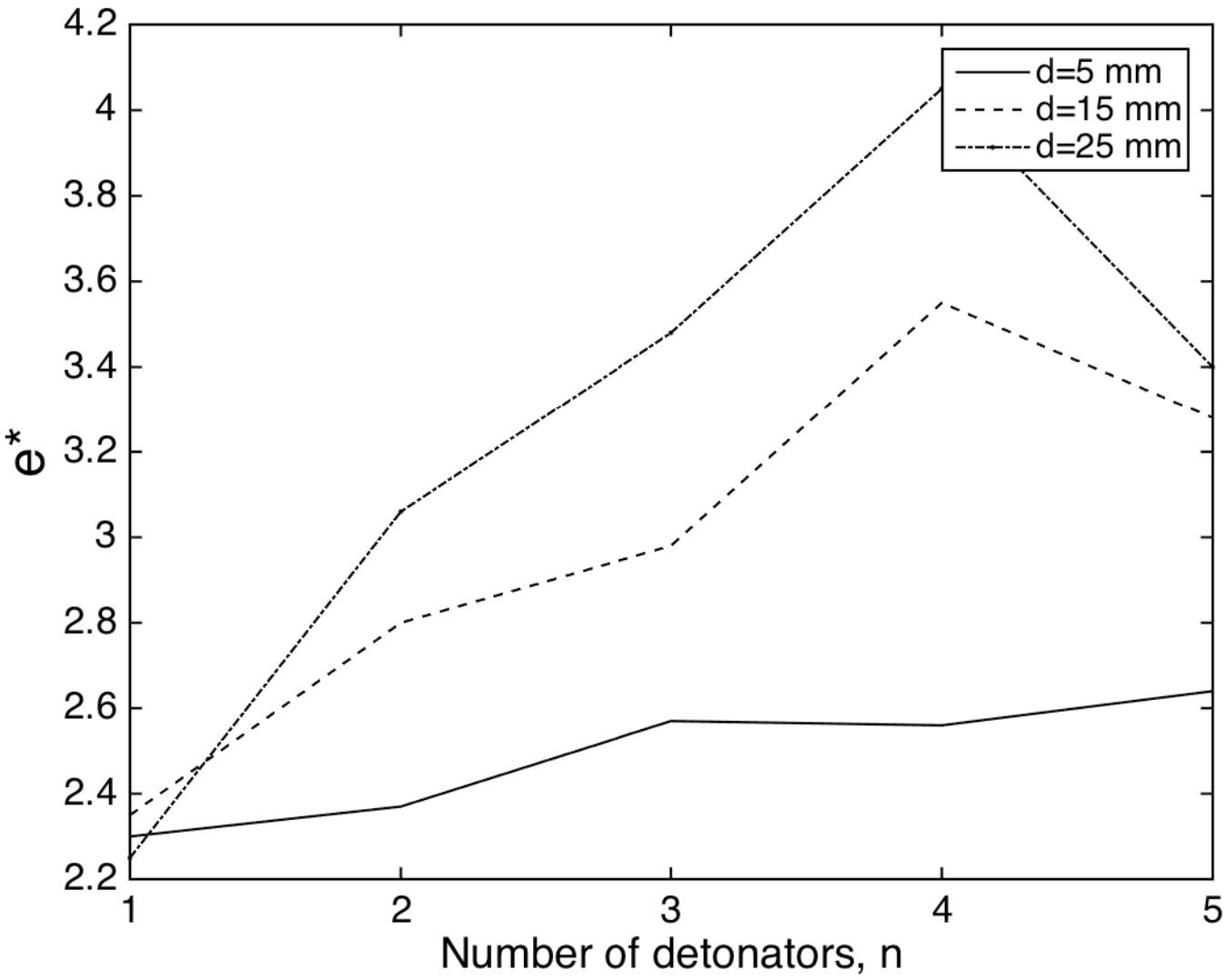
Figure 14b
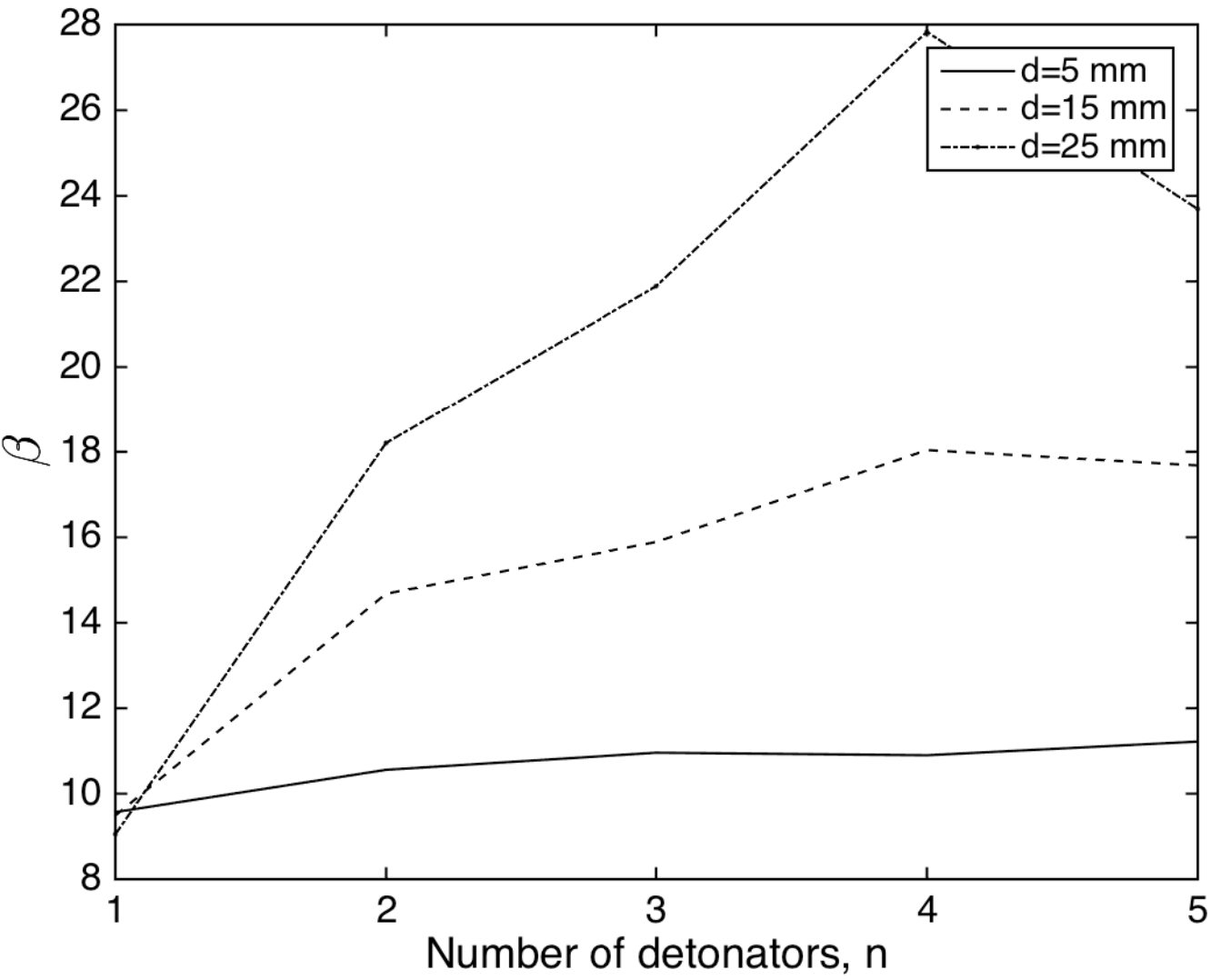
Figure 15a
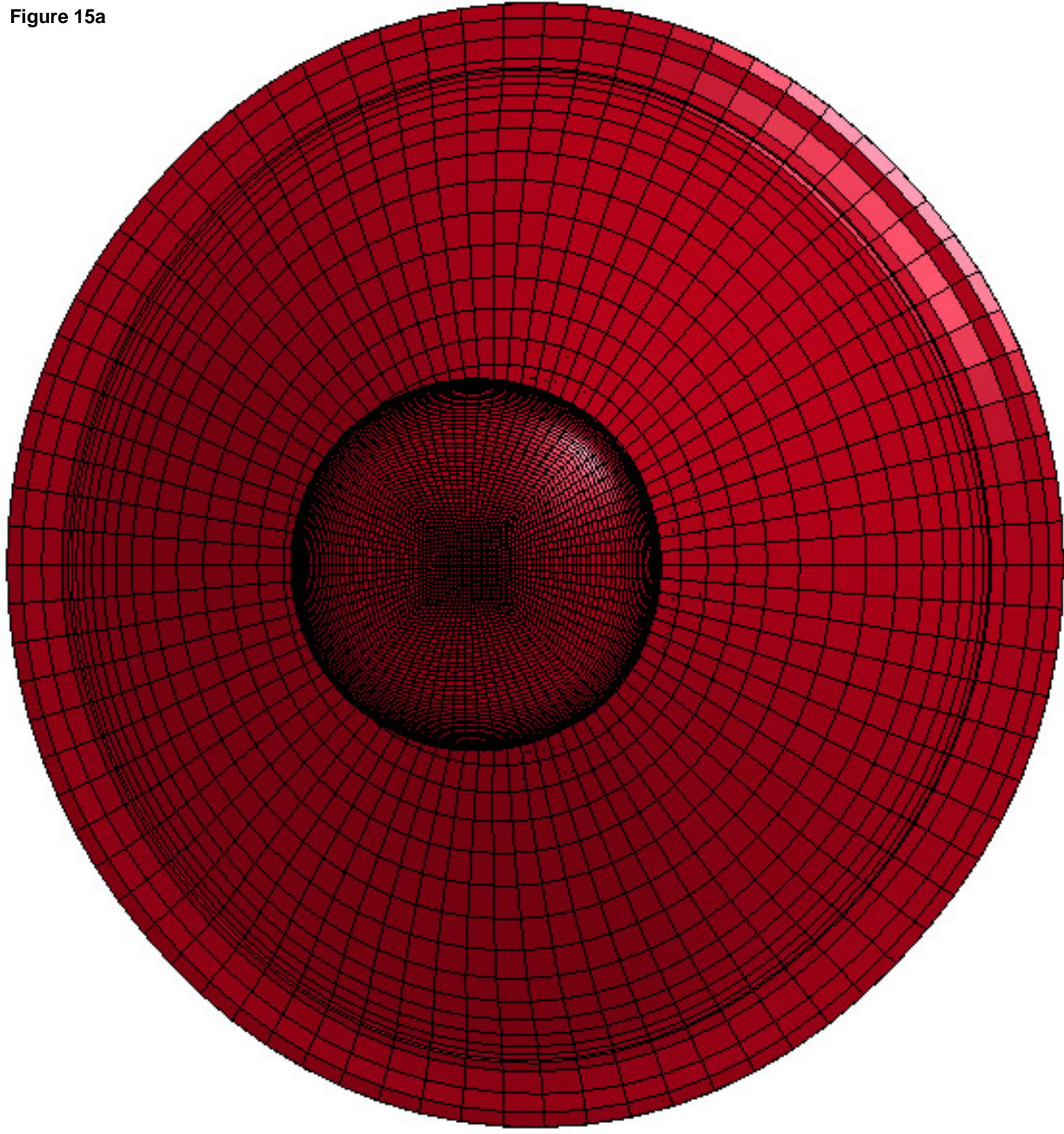
Figure 15b
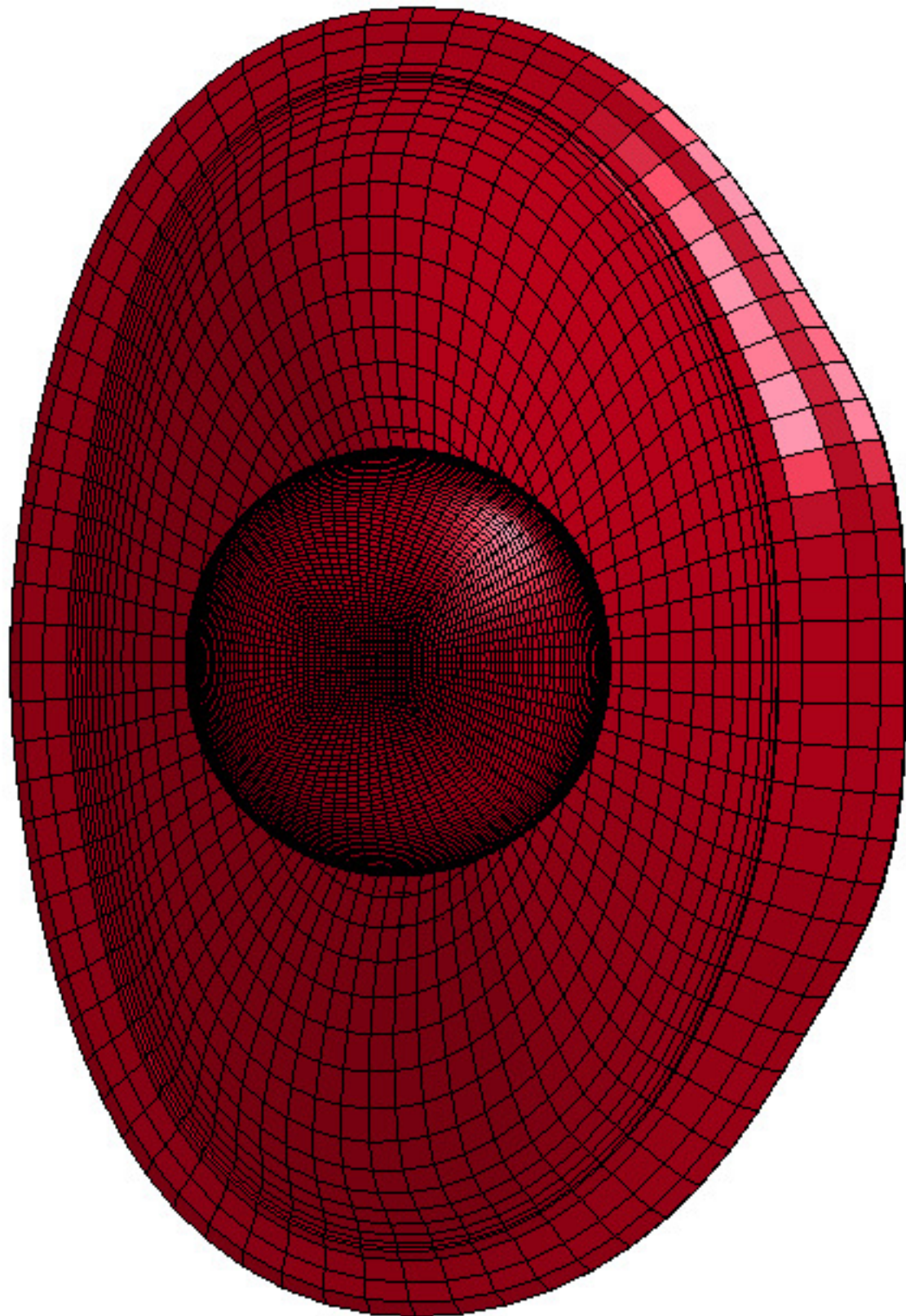
Figure 15c
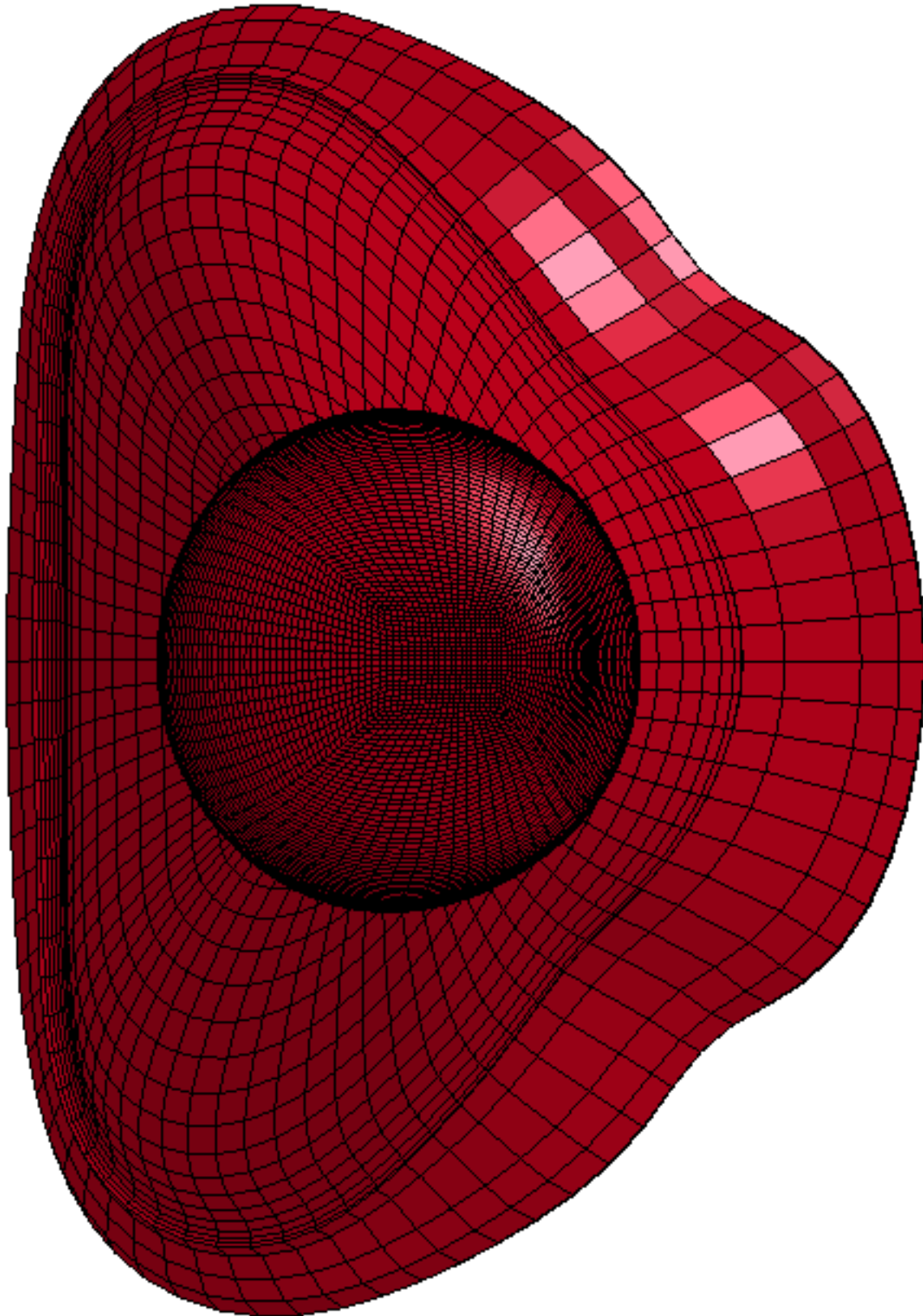
Figure 15d
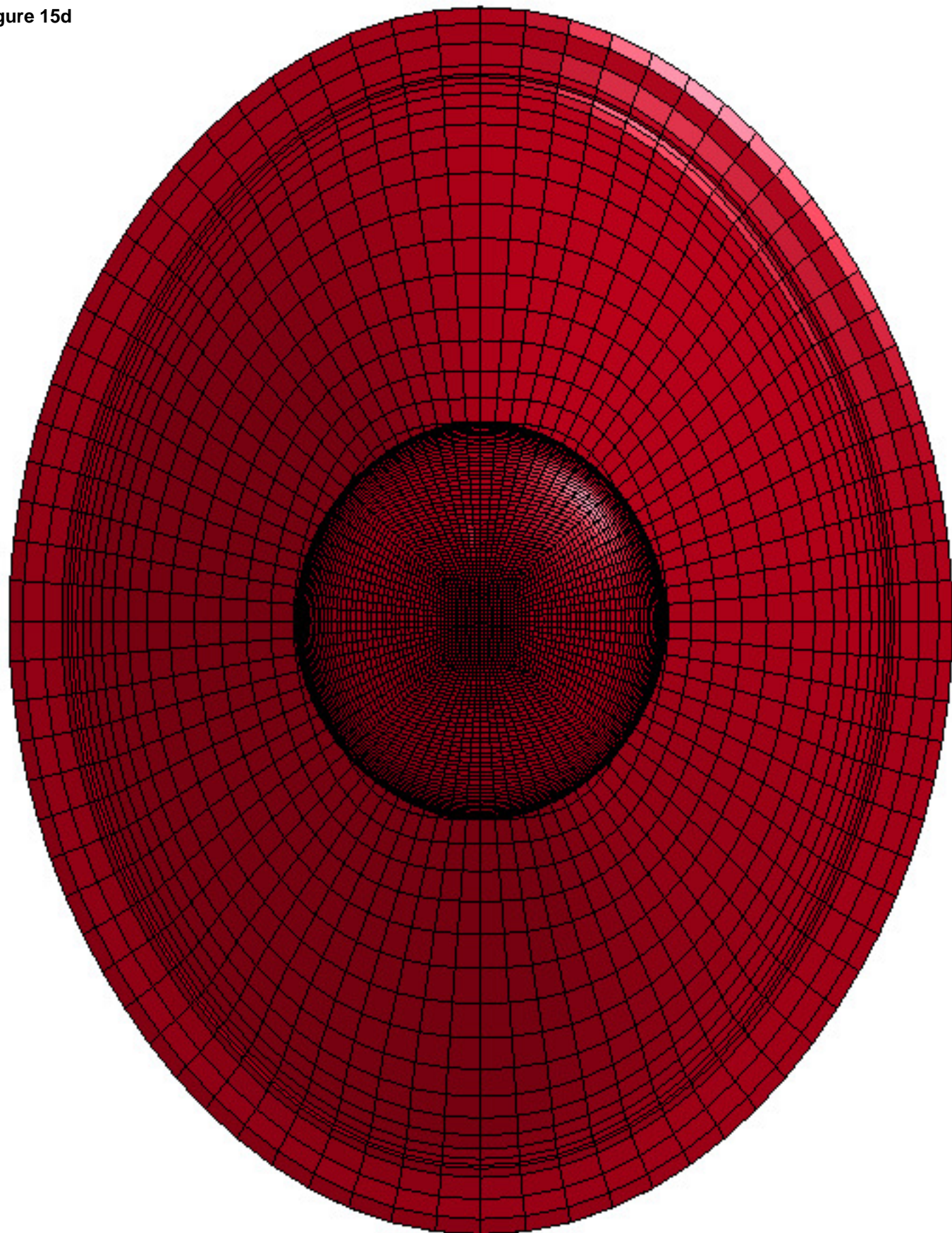
Figure 15e
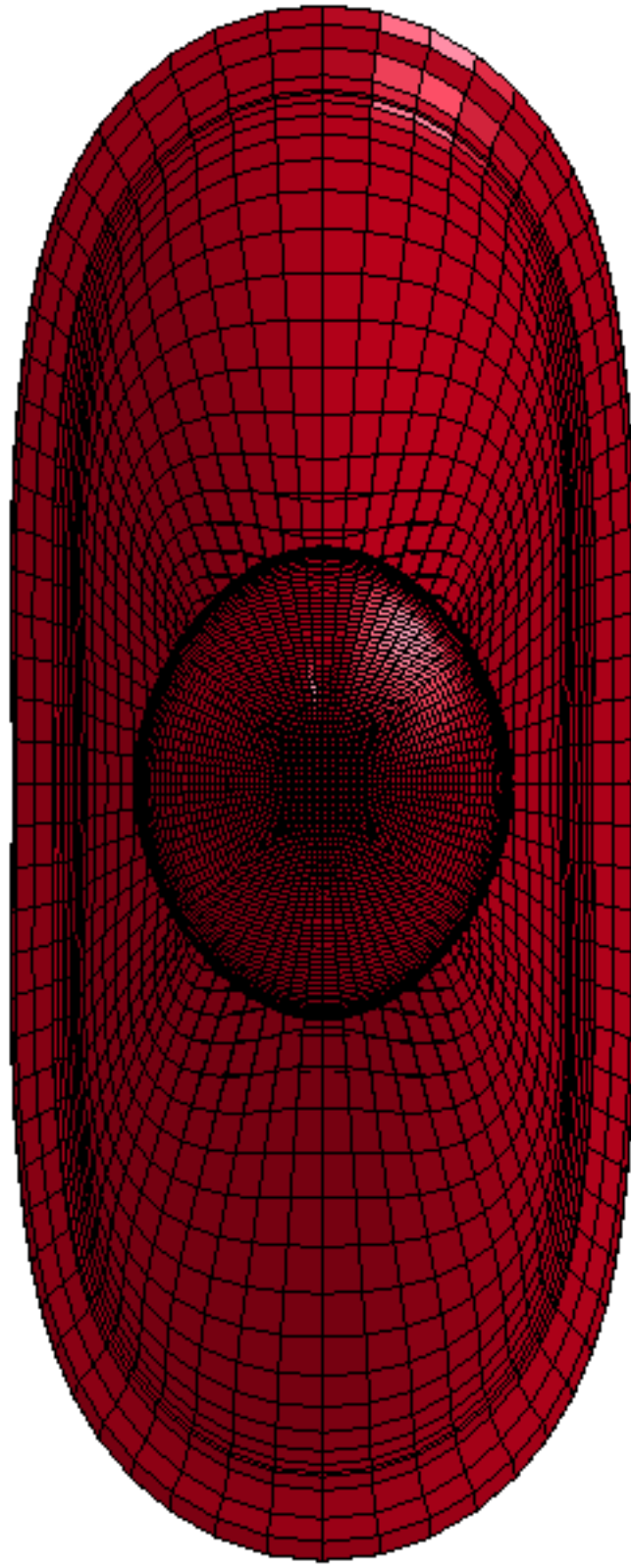
Figure 15f
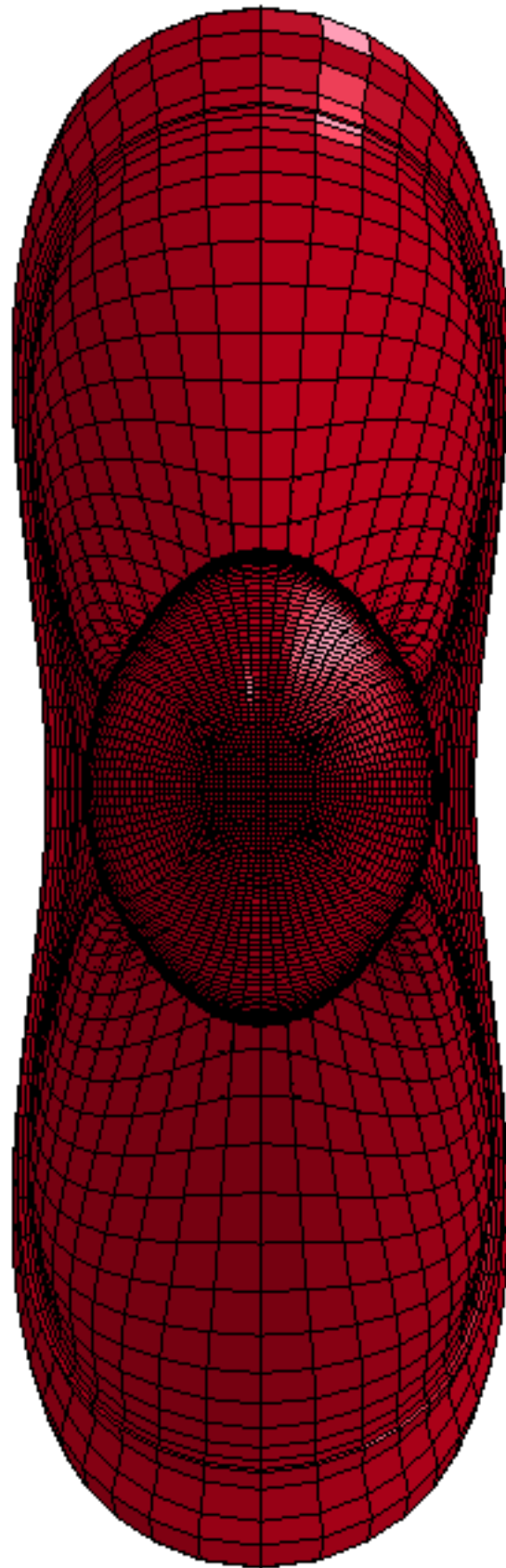
Figure 15g
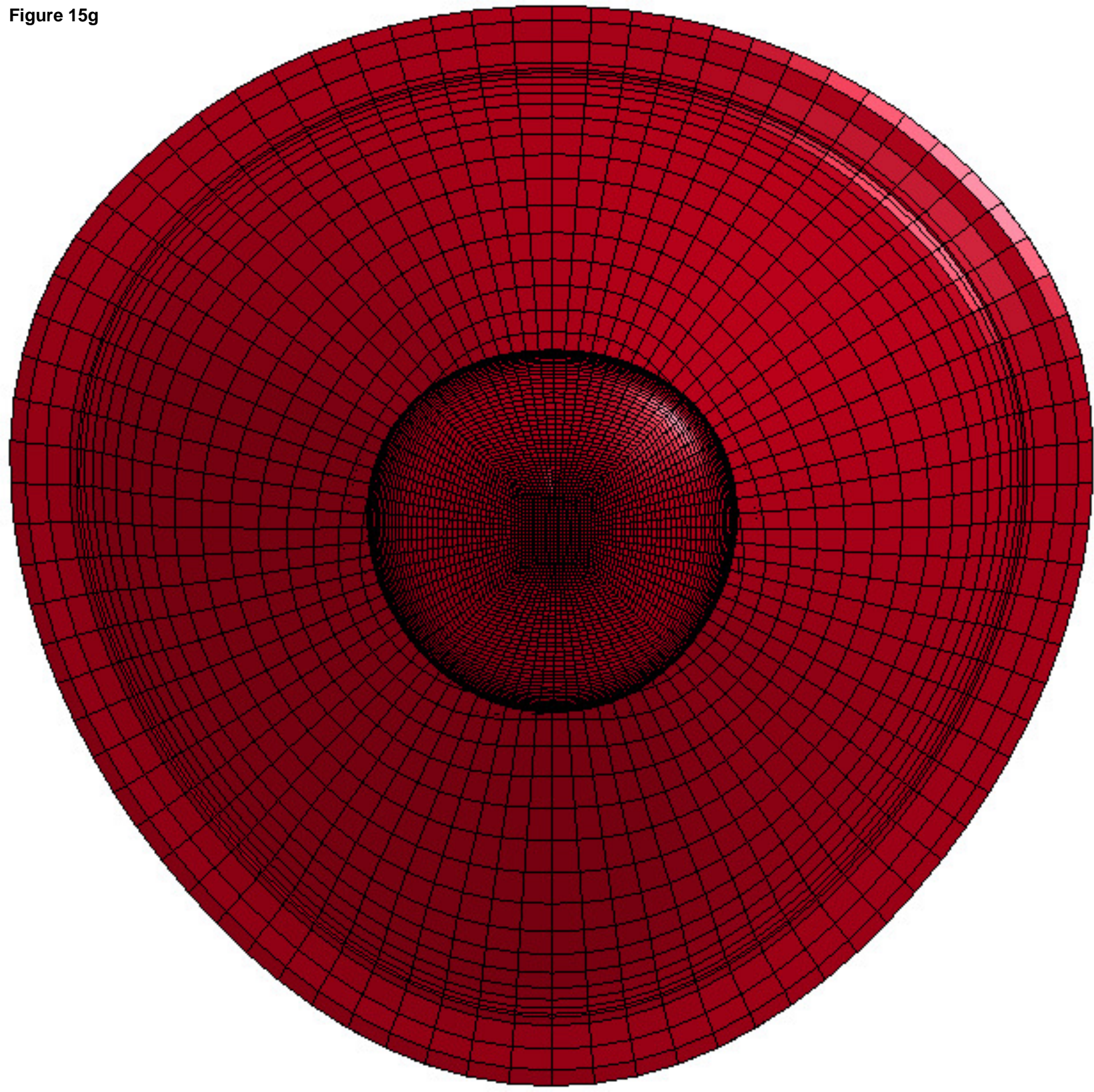
Figure 15h
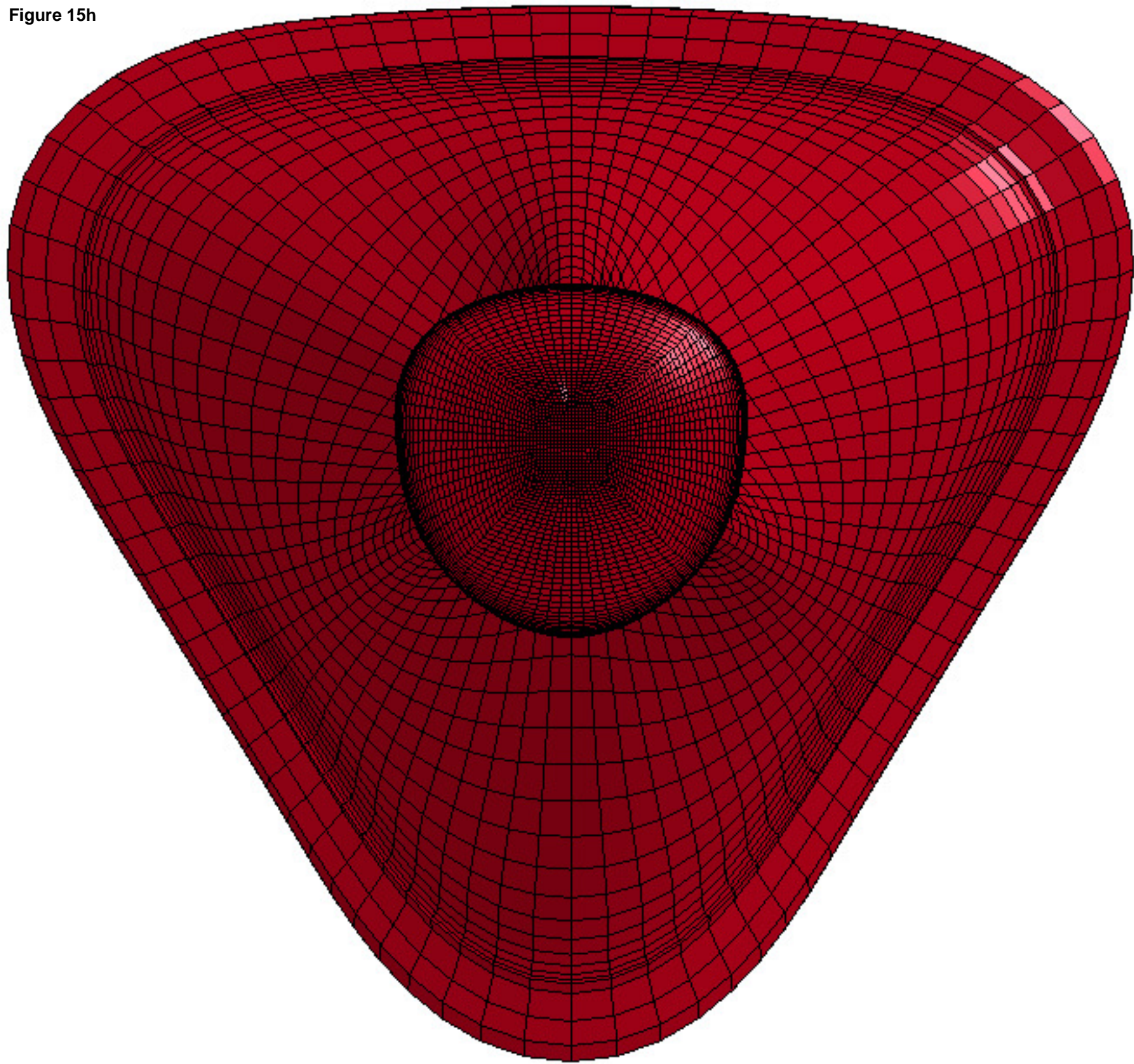
Figure 15i
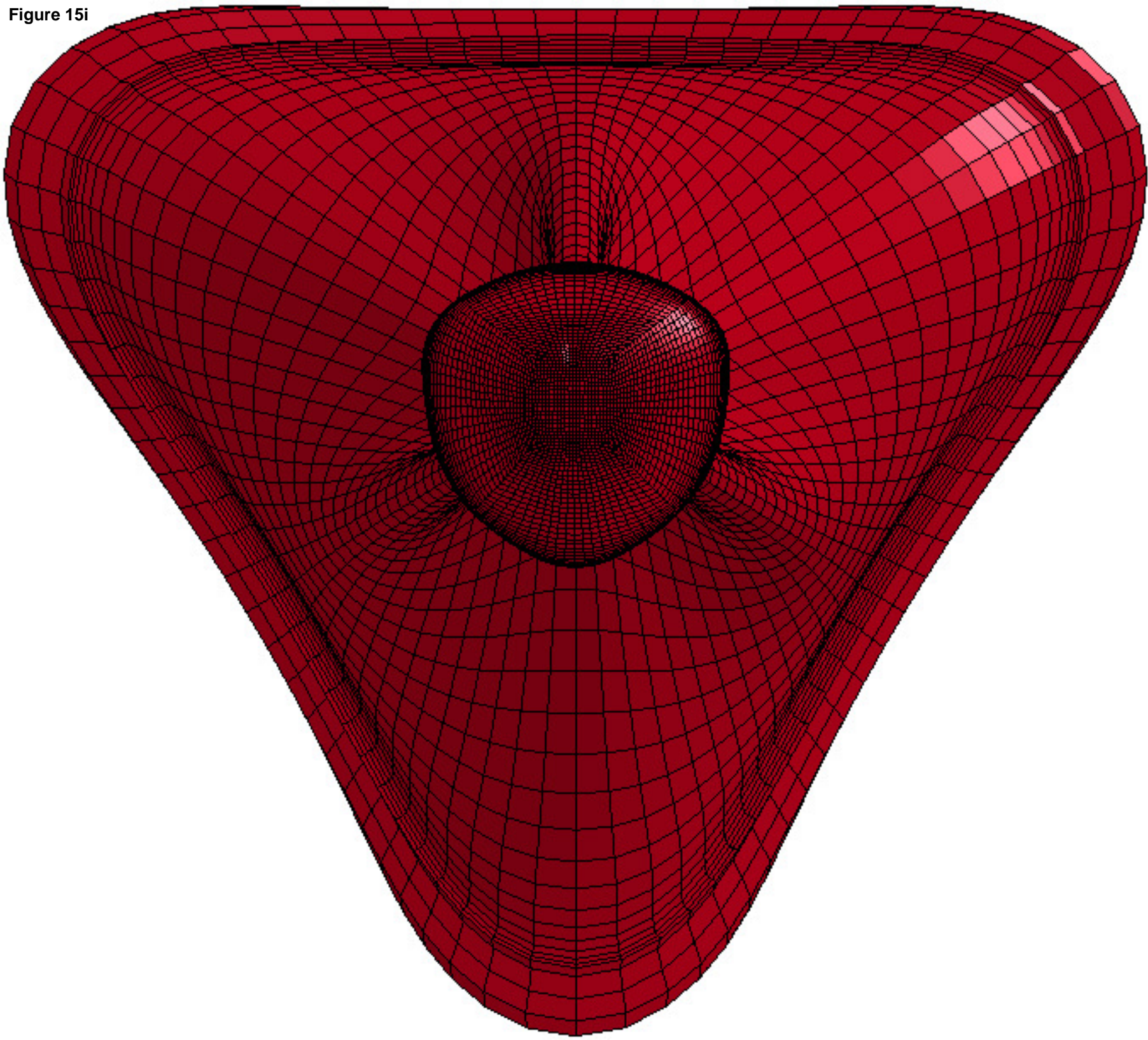
Figure 15j
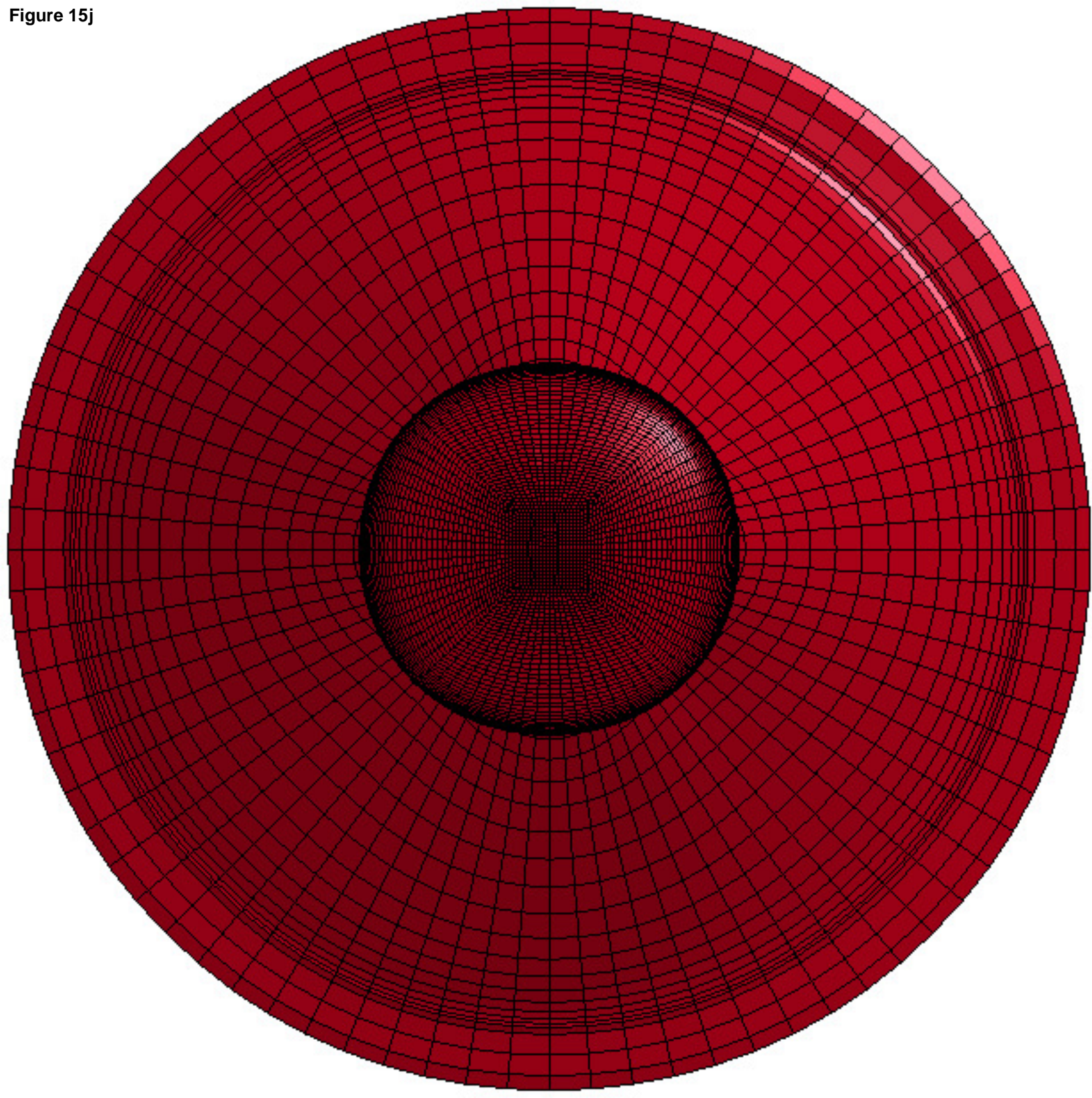
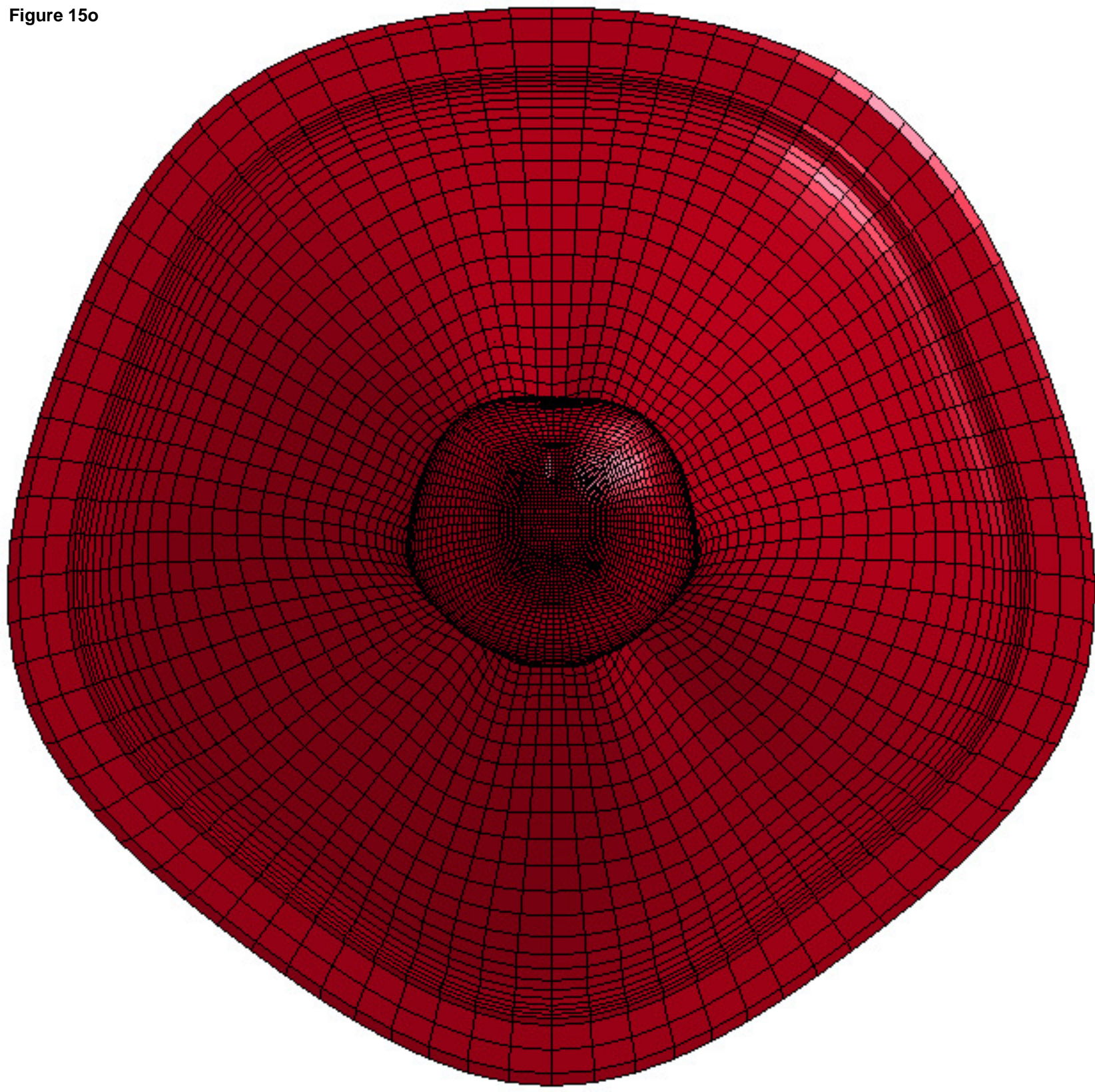Figure 15k
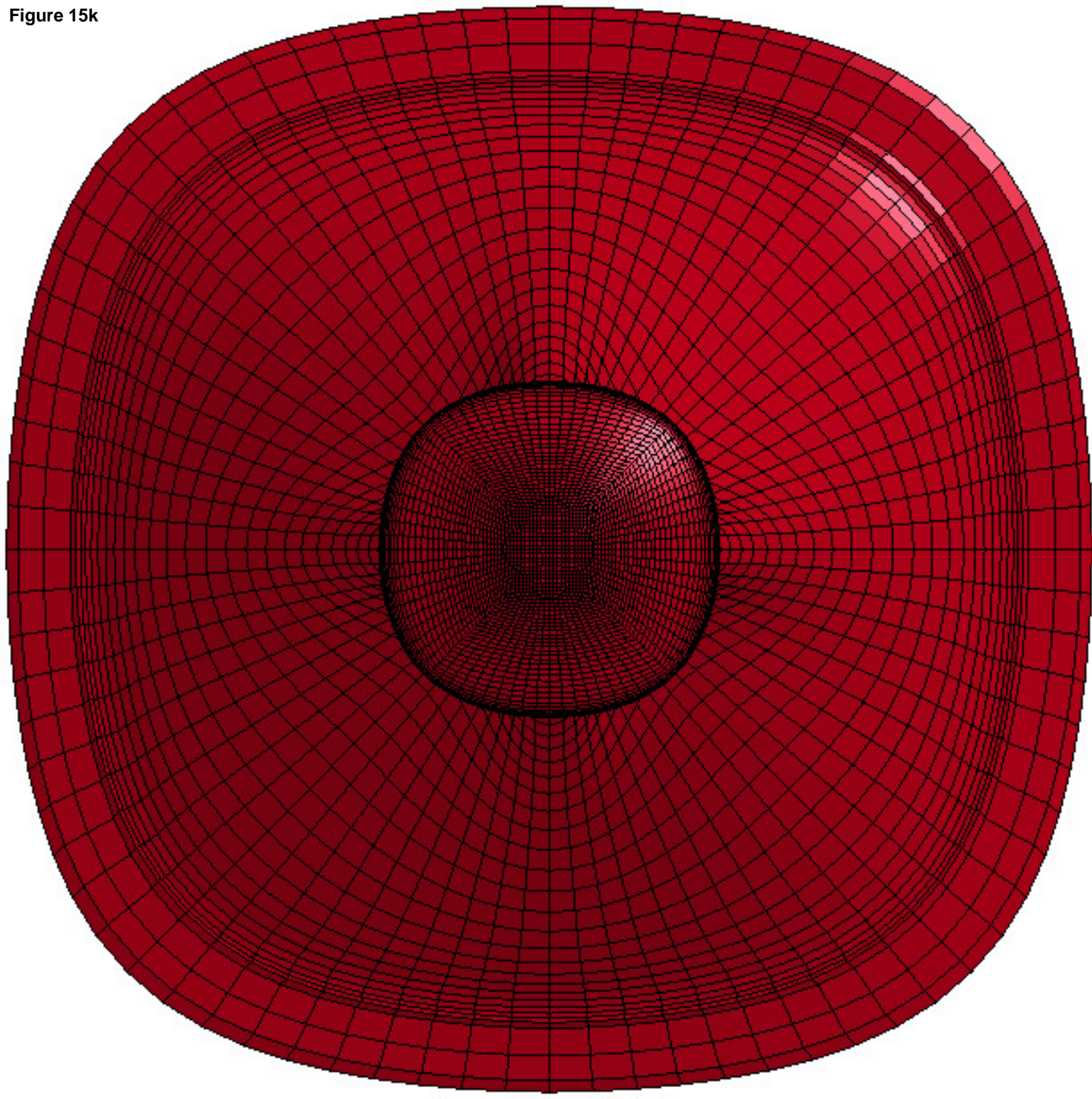
Figure 15I
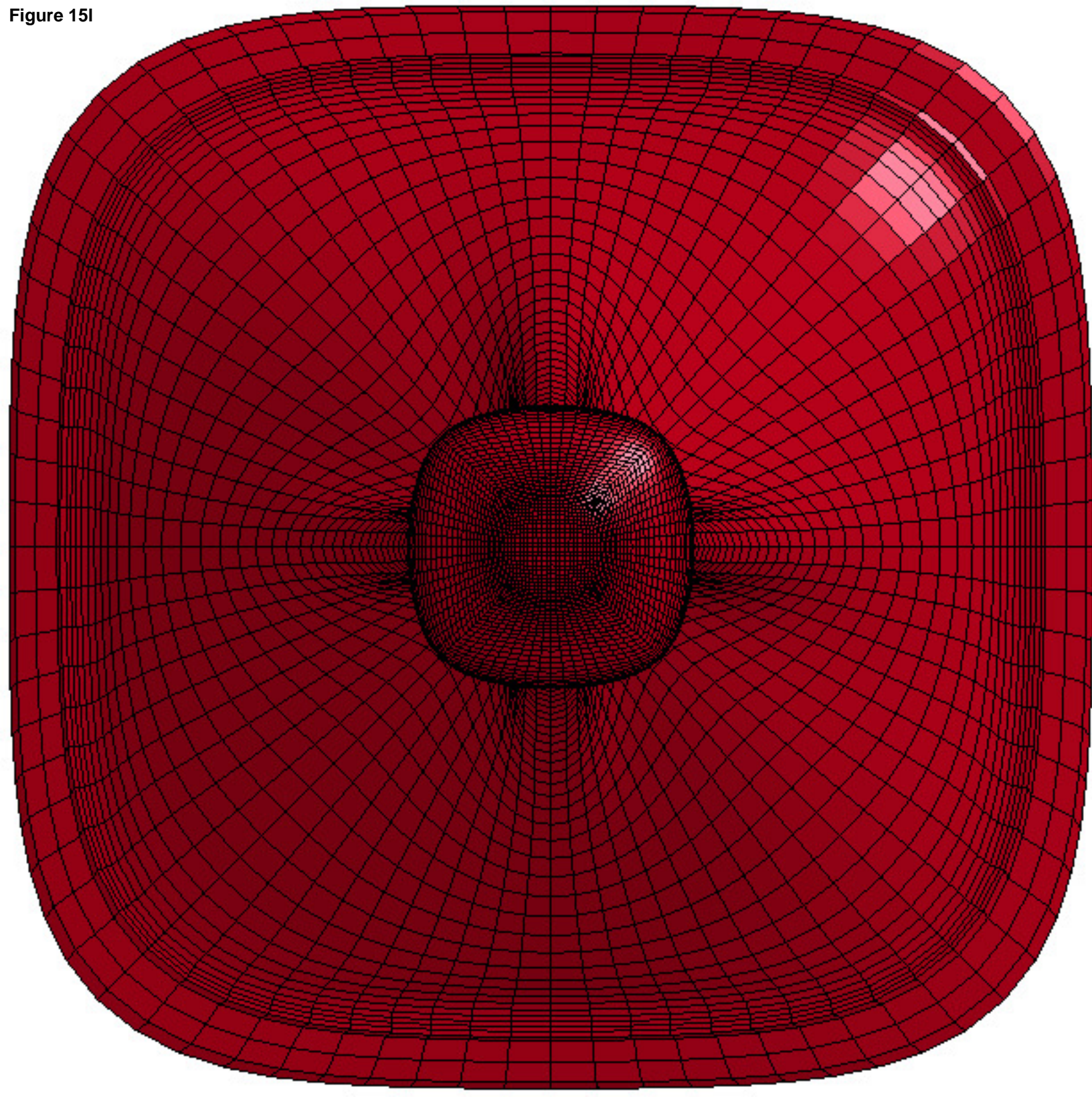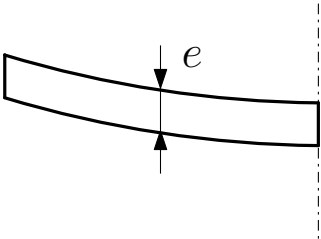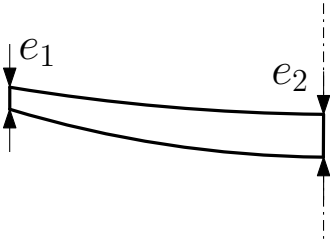
Figure 15m
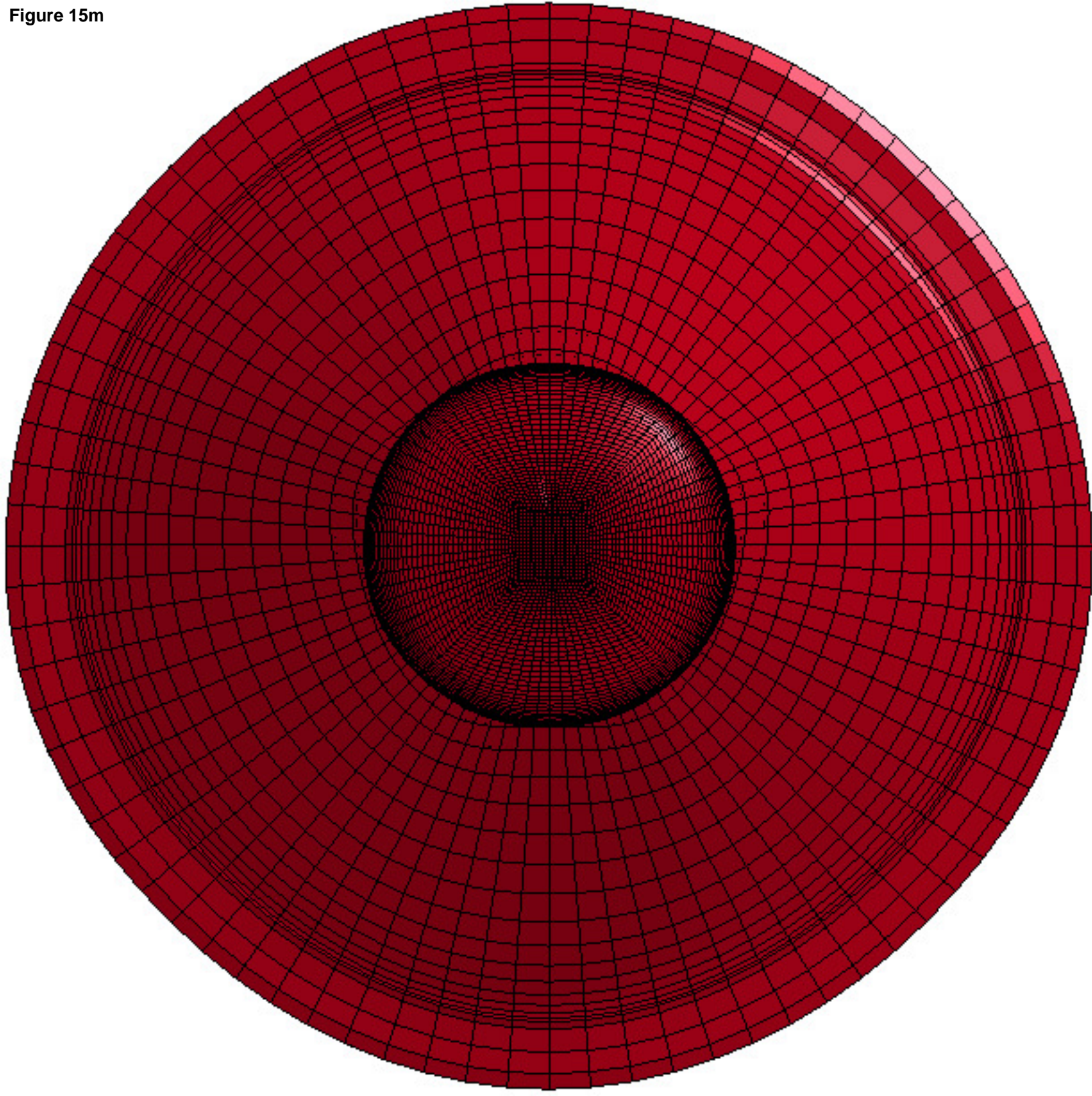
Figure 15n

Figure 15o

e_1

e_2
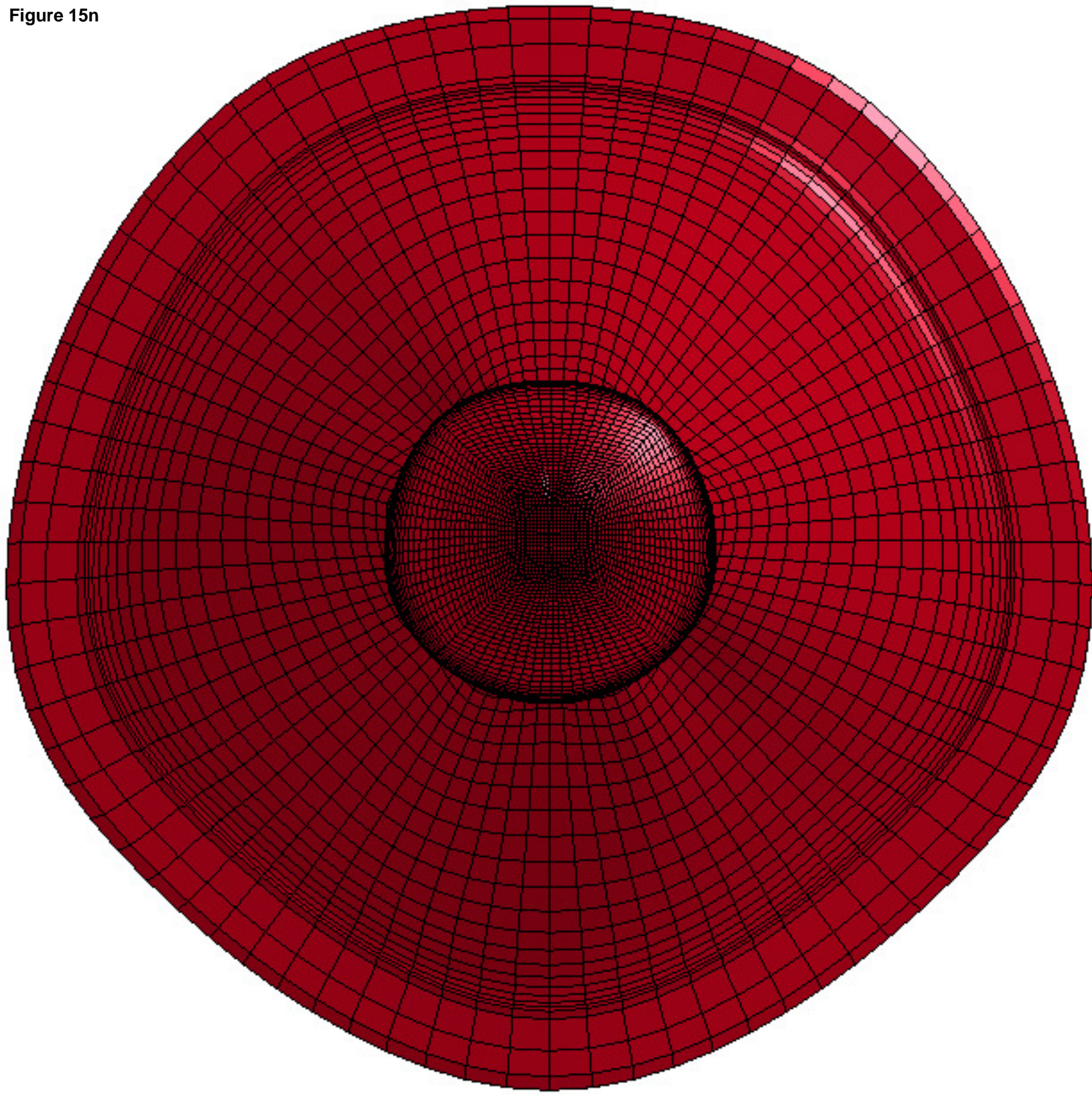
LaTeX Source Files

[Click here to download LaTeX Source Files: 20150601_DC-FTD_IJIE_LaTeX.zip](#)